Heliyon 9 (2023) e18644

Contents lists available at ScienceDirect

Heliyon

journal homepage: www.cell.com/heliyon

Assessment of the 1693 tsunami wave generation and propagation simulation based on multiple focal mechanism scenarios for recent disaster mitigation in eastern sicily, Italy

FX Anjar Tri Laksono [a,b]

[a] The Doctoral School of Earth Sciences, Department of Geology and Meteorology, Institute of Geography and Earth Sciences, Faculty of Sciences, University of Pécs, Pécs, Hungary
[b] Department of Geological Engineering, Faculty of Engineering, Jenderal Soedirman University, Purwokerto, Indonesia

ARTICLE INFO

Keywords:
Focal mechanism
Run-up
Propagation
Simulation
Tsunami

ABSTRACT

The 1693 tsunami was the most extensive earthquake-tsunami event in Sicily, submerging Catania, Augusta, and Syracuse. However, the earthquake rupture, water level, arrival time, and furthest inundation distance of the tsunami waves are not yet known. This study aims to investigate the tsunamigenic source, run-up height, furthest inundation distance, and arrival time of the 1693 tsunami waves on the east coast of Sicily. Moreover, the assessment of tsunami-prone zones was also conducted based on worst-case earthquake-tsunami scenarios. Numerical modeling was applied by proposing six offshore focal mechanism scenarios using the shallow water equation in Delft3D and Delft Dashboard. The input parameters include length, width, strike, dip, slip, rake, and depth of the earthquake rupture. Meanwhile, the tsunami wave propagation onshore utilized XBeach and ArcGIS, considering the maximum run-up height, surface roughness analyzed from land use maps, slope, river existence, and coastline from Digital Terrain Model (DTM) identification. The results indicate that the worst possible impact of the 1693 tsunami was generated by an earthquake with a magnitude of M_w 7.13. The maximum water level, furthest inundation distance, and arrival time achieved 7.7 *m*, 318 *m*, and 9 min after wave generation offshore, respectively. This simulation is consistent with the discovery of 1693 tsunami deposits at a distance of less than 400 *m* from the coastlines of Augusta and Syracuse, but it is above the estimated furthest inundation distance in previous studies, which only reached around 100 m–200 *m* from the eastern coastline of Sicily. The results of the study are reliable as they align with the 1697 historical document where seawater inundated San Filippo Square, Catania.

1. Introduction

The east coast of Sicily is a zone of high seismic intensity due to the Brucoli-Siracusa, Monterosso-Agnone, and Alfeo Etna Fault systems [1,2]. Historical records reveal that the eastern coast of Sicily experienced several earthquakes followed by tsunamis such as on July 21, 365, February 4, 1169, December 10, 1542, January 9 and 11, 1693, and December 28, 1908 (Fig. 1) [3–6]. As a consequence of these events thousands of people died and many properties and public facilities were destroyed [7,8]. Among several tsunami events that have occurred, the 1693 tsunami had the most severe impact on the eastern coast of Sicily due to its proximity to

E-mail address: anjar93@gamma.ttk.pte.hu.

https://doi.org/10.1016/j.heliyon.2023.e18644
Received 6 March 2023; Received in revised form 22 July 2023; Accepted 24 July 2023
Available online 27 July 2023

the tsunamigenic source and the large earthquake magnitude ($M_w > 7$) [9,10]. The epicenter of the 1693 earthquake was located off the coast of Ionian, eastern Sicily, while the epicenter of the 1908 earthquake was far from Catania, specifically in the Strait of Messina, which separates Calabria from Sicily [11–13]. Additionally, the magnitude of the 1693 earthquake (M_w 7–7.4) was greater than the 1908 (M_w 7.1) and 1169 (M_w. 6.6) earthquakes, hence increasing the likelihood of more significant post-shock impacts [6,10,14].

Several studies have been conducted to investigate evidence of paleotsunami deposits both onshore and offshore [3,17–22]. Six tsunami deposits were found in Augusta, of which two exhibit age correlation with the tsunami tragedies of 365 CE and 1693 [5,17]. Several boulders, weighing up to 182 t and covered with biogenic encrustations (serpulids, barnacles, lithophagas), are scattered along the coast between Augusta and Syracuse [10,23]. They were likely carried by the tsunami waves of 1169 CE, 1693, and 1908, which originated from the Ionian Sea and the Strait of Messina [10,23]. Three stratigraphic units in Ognina, southeastern Sicily, are associated with storms and tsunamis since the 4th century Common Era (CE) [14]. However, previous research has been unable to address the source of the tsunami or provide a comprehensive understanding of the 1693 tsunami waves that inundated the eastern coast of Sicily, including maximum water level, inundation distance, and arrival time of the tsunami waves. This issue is due to the lack of tsunami deposits from 1693 in Catania and limited data on earthquake ruptures that generated the tsunami. Understanding the inundation characteristics of the 1693 tsunami is crucial for enhancing disaster mitigation preparedness, especially considering that Catania and Augusta are the second-largest oil and gas import-export ports in Italy, popular tourist destinations, and densely populated areas in Sicily [24]. Through the simulation of multiple earthquake rupture scenarios and comparison with the evidence of tsunami deposits that have been found, it is possible to address the problems related to the tsunamigenic source, earthquake-tsunami magnitude, water level, inundation distance, and arrival time of the 1693 tsunami waves on the east coast of Sicily. This study will contribute to the mapping of tsunami-prone zones along the Catania-Syracuse area, based on the worst-case scenario of tsunami potential. To date, the 1693 tsunami remains the most severe tsunami event recorded along the east coast of Sicily [15,16,25], specifically between Catania and Syracuse. Furthermore, this study will contribute significantly as a reference in investigating the presence of tsunami deposits in Catania because, until now, no paleo-tsunami deposits similar to those found in Augusta and Syracuse have been discovered.

2. Materials and methods

2.1. Geological settings

East of Sicily towards the Ionian Sea is the Malta Escarpment. It is a steep submarine slope with a bathymetric of more than 3000 *m*, 300 km long, and 120 km wide [26–28]. Malta Escarpment is a transition zone between the continental and oceanic shelfs that separates two sectors of the African margin [29–33]. The Malta Escarpment extends south-eastward from the eastern coast of Sicily with a maximum slope gradient reaching 74° [28,34]. Currently, tectonic activity in the Malta Escarpment is categorized as slow vertical deformation rates [18,35–37]. The footwall block of the Malta Escarpment is locally known as the Hyblean Plateau and represents the emergence of a larger foreland domain. The Ionian Basin is east-dipping and the Hyblean continental promontory is west-oriented [38–42]. This transition zone is a paleo-tectonic remnant of the Permian-Triassic period during the opening of the Neo-Tethys which continued the spreading stage in the Jurassic-Cretaceous [29–33]. During the Pliocene-Quaternary, the Malta Escarpment discontinuity was reactivated by a normal-oblique extension [9,43]. Deformation in the Ionian Sea, off the southeast coast of Sicily is accommodated by a fault belt with a nearly *N*–S trend and consisting of three main fault segments, E-dipping, and a few

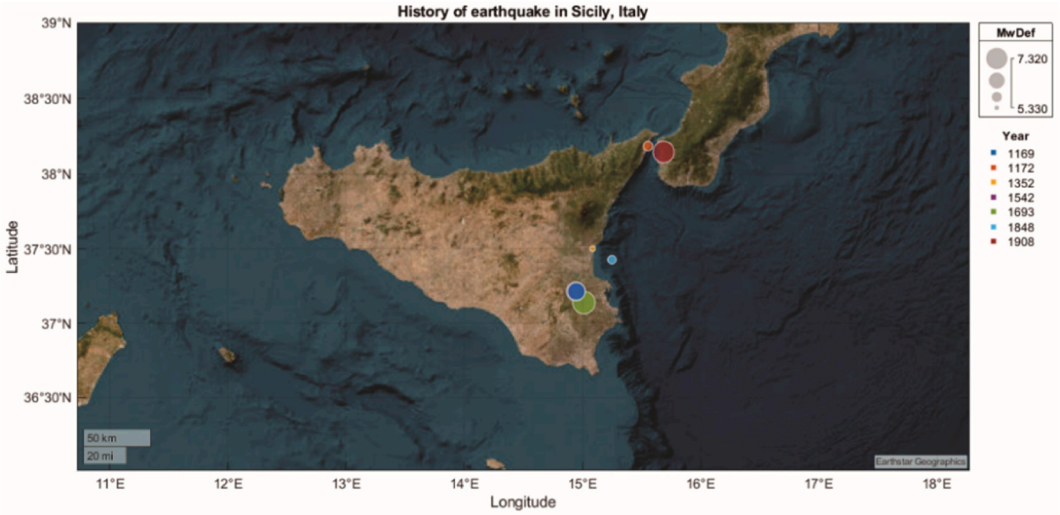

Fig. 1. Source records of earthquakes on the east coast of Sicily with magnitudes above M_w 5 from 1169 CE to 1908 CE. The earthquakes of 1169, 1542, 1693 and 1908 triggered tsunami waves [7,15,16].

oblique (right lateral) faults [9,44,45].

2.2. Tsunami history in eastern sicily

The east coast of Sicily has been hit by tsunamis several times, for example: July 21, 365, February 4, 1169, December 10, 1542, January 9 and 11, 1693, and December 28, 1908. The epicenter of the earthquake that caused the tsunami in 365 AD was located in the eastern Ionian Sea adjacent to Crete [3,5,8,14,46–49]. This tsunami not only damaged Greek territory but also along the eastern coast of Sicily, Italy [46,50,51]. The estimated magnitude of the earthquake-tsunami in 1169 was $M_{aw} = 6.6$ and inundated the coastal area around Messina and the Simeto River whose mouth is 20 km north of Augusta and 10 km south of Catania. The number of victims of this tsunami reached 25,000 people [17]. The earthquake that generated the tsunami in 1542 was estimated to have a magnitude of $M_{aw} = 6.6$, inundating the entire east coast of Sicily such as Catania, Augusta, and Syracuse with an area of about 6000 km^2 [12,25,52]

On January 9 and 11, 1693 earthquakes of magnitude $M_{aw} = 6.2$ and $M_{aw} = 7.4$ induced tsunamis and severe damage throughout eastern Sicily, the Aeolian and Mazzarelli Islands, and the Port of Marina in Ragusa, southern Sicily. The length of the inundated coast reached 230 km [51,53]. In Catania seawater flooded Mazzini Square and agricultural neighborhoods. In Syracuse after the earthquake, the seawater receded, followed by high waves that struck the whole of Syracuse. The same situation occurred in Augusta where the seawater receded before the tsunami waves arrived and flooded the harbor area up to San Domenico Monastery [17,54].

The magnitude of the 1908 earthquake in Messina reached $M_w = 7.1$ and was the most destructive earthquake in Italy during the 20th century [11,55]. Tsunamis struck southern Calabria, eastern and northern Sicily, and the region around the Sicily Channel up to Malta Island [48]. The length of the inundated Sicilian coastline was about 270 km [51]. Tsunami inundation in northeastern Sicily reached up to 250 *m* from the coastline. In Messina, the tsunami flooded the harbor and the fortress of St. Salvatore [17]. In Catania, the seawater rose up to 100 *m* from the shoreline and deposited algae, posidonie, madrepore and millepore fragments, molluscs and various fish. At the mouth of the Simeto River, seawater rose up to 700 *m* from the shoreline [5,17]. In Syracuse, after a fall in sea level immediately after the earthquake, the sea rose to 2 *m* above sea level. In the village of Brucoli, less than 10 km north of the city of Augusta, within 8 min of the earthquake shaking, the sea level dropped to 200 *m* from the shoreline seaward and then suddenly rose to 50 *m* from sea level landward [8,11]. In Augusta, the tsunami run-up height reached 1.75 *m* within 10 min of the first earthquake shaking. Outside the harbor area the run-up height was up to 2 *m* and dispersed 15 *m* from the shoreline. The average occurrence interval of tsunami events in eastern Sicily is about 250 years, but some scientists claimed approximately 400 years [25,46].

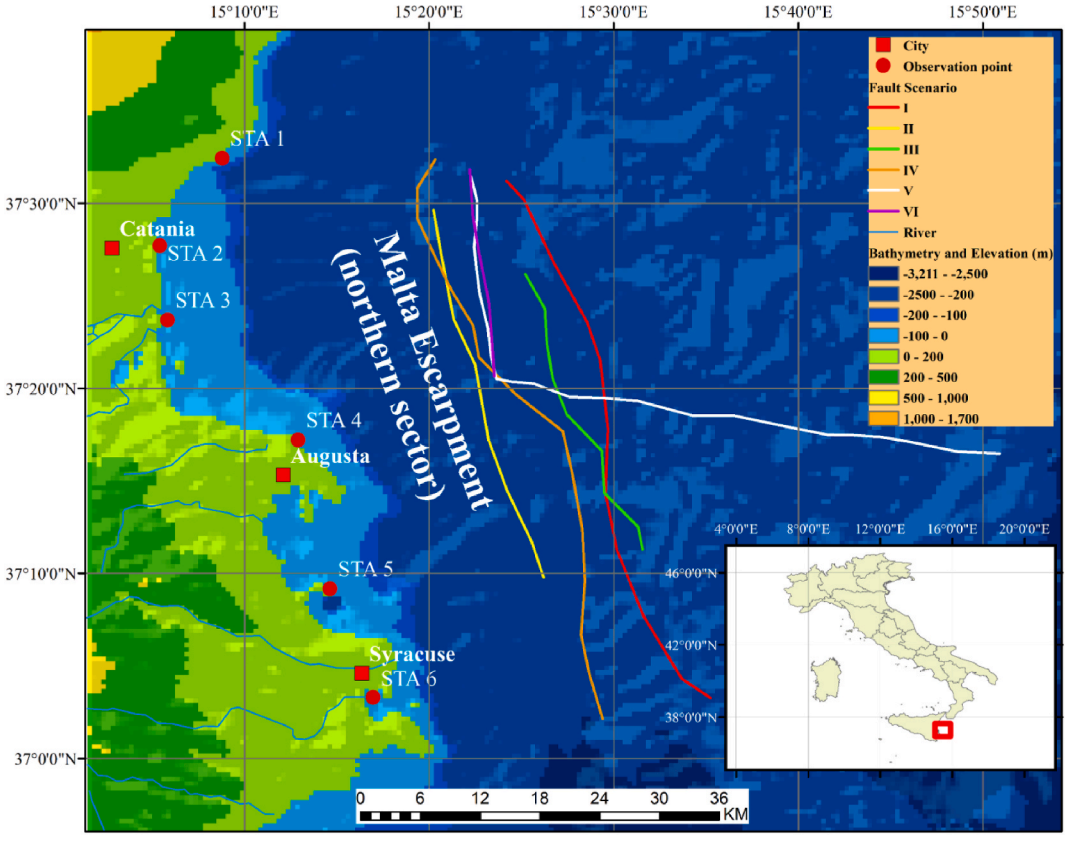

Fig. 2. Six tsunami wave heights were observed on the east coast of Sicily, three in the Catania and the others in Augusta and Syracuse. Six fault displacement scenarios were tested to determine the run-up height and inundation distance of the 1693 tsunami in Catania [4,9,11,56–59].

2.3. Data collection and methodology

Six tsunamigenic source scenarios were proposed in the 1693 tsunami simulation. The first scenario is the earthquake ruptures according to Argnani et al. [56] with a fault displacement of 42 km to the east of Catania. The second scenario is a fault movement that occurs at a distance of 30 km from Catania towards the Ionian Sea, with the fault parameters of Argnani et al. [4]. The third scenario involves the fault parameters proposed by Gallais et al. [57], where the fault displacement is located in the Ionian Sea, 36 km east of Catania. The fourth scenario represents a tsunamigenic source based on fault parameters of Gambino et al. [9], which is located 24 km to the east of Catania. The fifth scenario utilizes the fault parameters proposed by Okada [58,59], where the fault extends NNW–SSE and then changes direction to E–W at Augusta. Lastly, the sixth scenario involves the earthquake rupture proposed by Monaco and Tortorici [11], where the fault displacement occurs only along the east of Catania and is discontinuous towards Augusta or Syracuse (Fig. 2). Six observation sites were selected as reference points in the investigation of the maximum run-up height and arrival time of tsunami waves in the nearshore. Three observation points are located in Catania and the others are situated between Augusta and Syracuse (Table 1 and Fig. 2).

The tsunami flow simulation was divided into two, namely reconstructing tsunami wave propagation offshore and defining tsunami flow and inundation on land. The simulation of tsunami wave propagation onshore and offshore employed Delft Dashboard and Delft3D Flow, while tsunami flow and inundation onshore combined the XBeach model with ArcMap and ArcScene. Delft Dashboard is a hydrodynamic numerical modeling program developed to integrate the Delft3D Flow model with the XBeach model. This application could solve linier (equations **(1)**, **(2)**, **(3)**, and **(4)**) and non-linear (equations **(5)** and **(6)**) shallow water equation problems in the area bounded by a grid using a finite difference scheme [60–63].

$$\frac{\partial \eta}{\partial t}+\frac{1}{R\ cos\ \varphi}\left\{\frac{\partial P}{\partial \psi}\ (cos\ \varphi\ Q)\right\}=-\frac{\partial h}{\partial t} \tag{1}$$

$$\frac{\partial P}{\partial t}+\frac{gh}{R\ cos\ cos\ \psi}\ \frac{\partial \eta}{\partial \psi}-f\ Q=0 \tag{2}$$

$$\frac{\partial P}{\partial t}+\frac{gh\partial \eta}{\partial \psi}+fP=0 \tag{3}$$

$$f=\Omega\ sin\ \varphi \tag{4}$$

$$\frac{\partial P}{\partial t}+\frac{1}{R\ cos\ \varphi}\ \frac{\partial}{\partial \psi}\left\{\frac{P^2}{H}\right\}+\frac{1}{R}\ \frac{\partial}{\partial \varphi}\left\{\frac{P\ Q}{H}\right\}+\frac{g\ H}{R\ cos\ \varphi}\ \frac{\partial \eta}{\partial \psi}-f\ Q+Fx=0 \tag{5}$$

$$\frac{\partial Q}{\partial t}+\frac{1}{R\ cos\ \varphi}\ \frac{\partial}{\partial \psi}\left\{\frac{P\ Q}{H}\right\}+\frac{1}{R}\ \frac{\partial}{\partial \varphi}\left\{\frac{Q^2}{H}\right\}+\frac{g\ H}{R\ cos\ \varphi}\ \frac{\partial \eta}{\partial \psi}-f\ Q+Fx=0 \tag{6}$$

Where:η: water elevation (m)P: the volume flux components in the xQ: the volume flux components in the yφ: Latitudeψ: LongitudeR: radius of earthg: gravityh: water depth: Coriolis force coefficientΩ: the rotation of earth.

The characteristics of wave propagation in shallow water and deep water are very different, therefore the grid resolution applied is also different. When tsunami waves are generated offshore, the wave amplitude is smaller than the wavelength. However, as the wave propagation approaches the shoreline where the depth of the water body turns shallower, the amplitude of the wave rises, while the wavelength becomes shorter [62,64,65]. Therefore, the amplitude of tsunami waves at the coast is more significant than their wavelength. This indicator affects the change in wave rates offshore and when it touches land. The tsunami wave rate in offshore is more rapid than when it arrives at the coast, but the wave height in offshore is lower than in onshore [62,66,67]. In this study, the grid resolution implemented offshore was 2 $m \times 2\ m$, while the onshore grid resolution was 1 $m \times 1\ m$.

We compared the Gebco 19 bathymetry which has a resolution of 500 m with the EMODnet Adriatic Sea-Ionian Sea-Central Mediterranean resolution of 125 m. We choose Riemann as the boundary type in the flow condition setting because when the generated wave has achieved the maximum boundary, it will be reflected back and the same process will occur again [12]. The forcing type chosen is time-series with gravity values of 9.81 m/s^2, water density of 1025 kg/m^3 for seawater, air density of 1.15 kg/m^3, and manning roughness coefficient of 0.024. The numerical parameter settings adopted minimum depth at grid cell centers and mean

Table 1
The six observation points are located at a depth of 10 m, extending from Catania to Syracuse.

Observation	Latitude	Longitude	Depth (m)
STA 1	37.5347	15.1288	10
STA 2	37.4595	15.0886	10
STA 3	37.3892	15.0936	10
STA 4	37.3898	15.0937	10
STA 5	37.2896	15.2139	10
STA 6	37.1500	15.283	10

depth at grid cell faces, threshold depth 0.1 *m*, and flood advection scheme for momentum to visualize the tsunami inundation on the main land in detail.

We used TPXO 8.0 global inverse tide model and Fourier analysis with maximum water level parameters to visualize the wave propagation over the continental shelf. The conversion of the media descriptor file (mdf) format from Delft Dashboard to DAT file was executed within Delft3D Flow. We displayed the simulated tsunami propagation in three-dimensional form and graphed the tsunami run-up height at each observation point during the specified time interval with Delft3D-QUICKPLOT. The correlation information between wave propagation time and elevation from Delft3D Flow was inputted into ArcScene to visualize the tsunami flow propagation in the coastal area of Catania.

A digital terrain model (DTM) map with 10 *m* resolution as basemap was obtained from National Institute of Geophysics and Volcanology (INGV). To retrieve the morphological features when the 1693 tsunami event occurred, we took into account the vertical land movement collected from previous studies such as [14,35,68,69], erosion and accretion rates of the Catania coastline according to Laksono et al. [70], and relative sea-level change derived from Lambeck et al. [68], Scicchitano et al. [18], and Anzidei et al. [71]. Validation of the simulated inundation distance and run-up height of tsunami waves on shore was undertaken by comparing the evidence of tsunami deposits by De Martini et al. [17], Barbano et al. [23], and Scicchitano et al. [10].

After the stage of estimating the impact of past tsunamis, the next step is to determine the maximum inundation distance from the modern coastline using XBeach by inputting the elevation, time, and run-up height parameters obtained from the Delft3D and Delft Dashboard simulations. The output from this stage is adopted as the basis for simulating tsunami propagation on land in ArcGIS. We utilized the Fuzzy membership method to classify the tsunami hazard zones in the study area. The input parameters for the Fuzzy membership are the values of tsunami height loss per 1 *m* of inundation distance (H_{loss}) obtained from equation **(7)** [72]. The calculation of H_{loss} (equation **(7)**) takes into account the manning roughness coefficient (Table 2), slope, wave height, and coastline. The Manning roughness coefficient is retrieved from the land use surface coefficient values, the wave height input is in accordance with the Delft Dashboard and Delft3D simulations. The coastline of the eastern coast of Sicily was obtained from the latest coastline position research conducted by Laksono et al. [70,73].

$$H_{loss} = \left(\frac{167n^2}{H_0^{\frac{1}{3}}}\right) + 5\ sin\ S \tag{7}$$

Where:H_{loss} = tsunami height loss per 1 *m* of inundation distance (m)N = manning roughness coefficientH_0 = maximum wave height upon reaching the shoreline (m)S = slope (radian).

3. Results

3.1. Simulation of tsunami wave run-up height and propagation

3.1.1. Scenario 1

The magnitude of the earthquake likely to be generated from the Scenario One simulation is M_w 7.11. This scenario, adopting the fault displacement of Argnani et al. [56] (Fig. 3 and Table 3), indicated that at observation point 1, the maximum height of the tsunami run-up was about 0.39 *m*, which occurred within 12 min after the first wave formed offshore (Fig. 4 A). The time span of the arrival of the first wave is similar to that of observation point 2 (Fig. 4 B). However, at observation point 2, the height of the first wave run-up attained 1.75 m (Fig. 4 B) and then gradually dropped to 1 *m* at the 36th minute, 0.75 *m* at the 58th minute, 0.48 *m* at the 72nd minute, and 0.4 *m* at the 75th minute. At observation point 3 (Fig. 4C) located at the mouth of the Simeto River, the maximum run-up height of 3.3 *m* was recorded 16 min after wave generation. Subsequently, the wave height gradually diminished to 2.1 *m* by the 25th minute. At the 43rd minute a second wave with a run-up height of 1.7 *m* was detected at observation site 3, after which the wave height gradually subsided and returned to normal. At observation stations 4, 5, and 6, the maximum run-up heights were 4.4 m (Figs. 4 D and Fig. 5 A), 3.25 *m*, and 0.68 *m* within 7 min, 9 min, and 15 min, respectively. At observation station 4, the wave height above 1 *m* lasted for about an hour which then decreased to below 1 *m*. Meanwhile, at observation site 5 (Fig. 4 E), waves with a height of more than 1 *m* occurred for about 50 min which then became less than 1 *m* in the following minute. At STA 6 (Fig. 4 F) the maximum run-up height of 0.68 *m* occurred at the 15th minute after the formation of the first tsunami wave at the earthquake source. According to the tsunami simulations in Fig. 5 A and B, the maximum run-up heights in Augusta and Syracuse occurred at the 7th minute after tsunami wave generation while in Catania the highest water level was observed after 12 min of tsunami formation. Based on the records of wave

Table 2
Manning surface roughness coefficient for each land use type according to Berryman [74].

Land use type	Manning roughness coefficient
building	0.08
vegetation	0.07
wetland vegetation	0.025
rice/grass	0.02
bare land	0.015
Water body	0.007

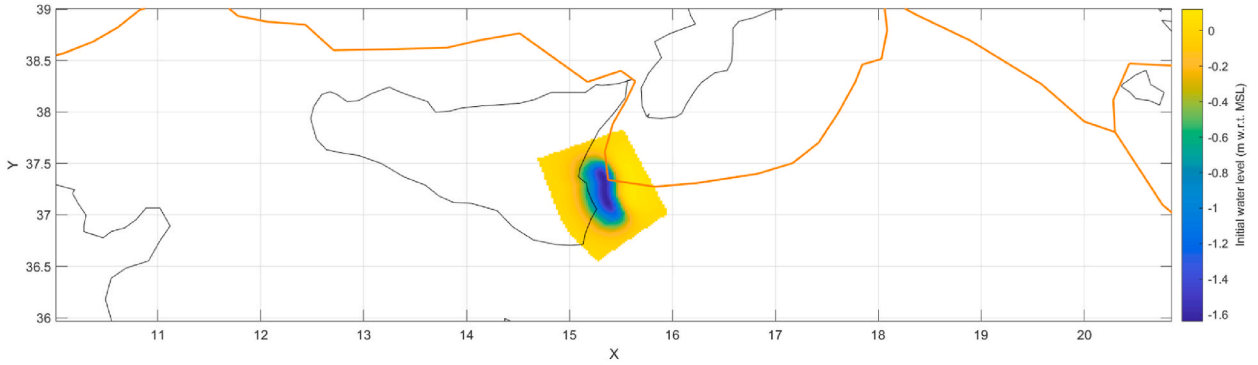

Fig. 3. Earthquake rupture and tsunami wave generation location in Scenario 1. The length of the fault displacement reaches 56.7 km.

Table 3
Earthquake rupture and fault parameters in Scenario 1. The magnitude of the earthquake generated by the scenario 1 simulation was Mw 7.11 [56].

Fault parameter	Rupture input	Magnitude of earthquake (M_w)
Strike (°)	~N139E–N181E	7.11
Dip (°)	49	
Length (km)	56.7	
Width (km)	26.7	
Rake (°)	270	
Slip (m)	5	
Depth (km)	20	

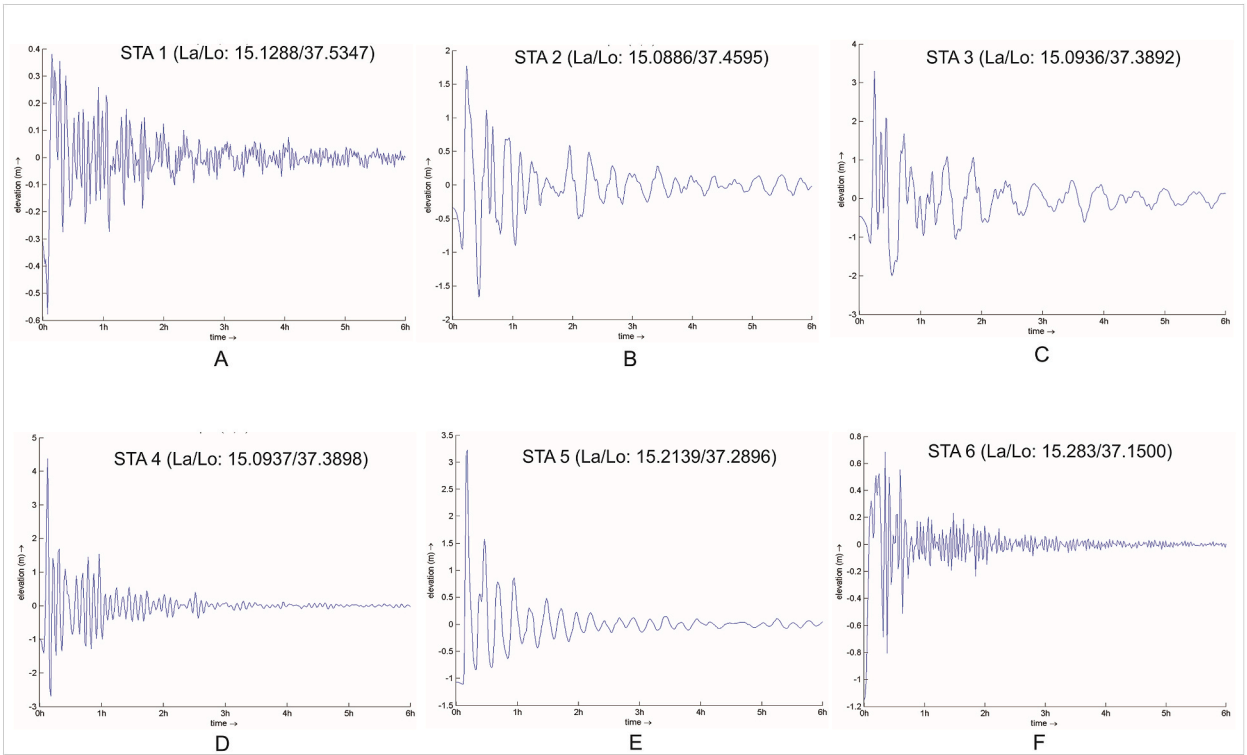

Fig. 4. Six graphs depicting the relationship between propagation time (x-axis) and tsunami run-up height (y-axis). The maximum run-up heights at A. STA 1, B. STA 2, C. STA 3, D. STA 4, E. STA 5, and F. STA 6 are 0.39 *m*, 1.75 *m*, 1.7 *m*, 4.4 *m*, 3.25 *m*, and 0.68 *m*, respectively.

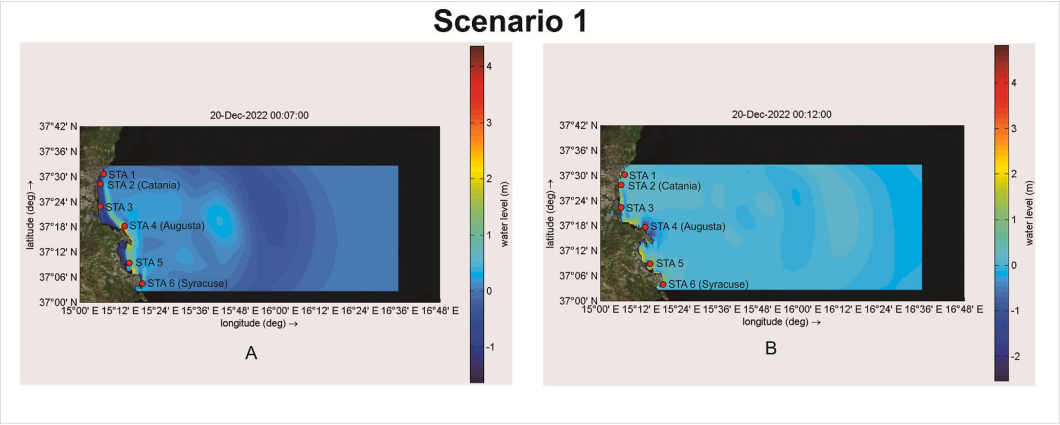

Fig. 5. Image showing the tsunami wave propagation offshore until it reached the east coast of Catania, Augusta, and Syracuse. A. At the 7th minute, the run-up height at Augusta (STA 4) stood at 4.4 *m*. B. In Catania, a wave height of 1.75 *m* occurred after 12 min of tsunami wave generation.

propagation time and run-up height as depicted in Fig. 4 A, B, C, D, E, and F and Fig. 5 A and B, the maximum run-up height and arrival time of tsunami waves at each observation location are given in Table 4.

3.1.2. Scenario 2

The earthquake magnitude derived from the simulation of the amended fault displacement parameters of Argnani et al. [4] is M_w 6.81 (Fig. 6 and Table 5). Fault displacement scenario 2 at observation point 1 has not generated significant wave heights, in fact the maximum height is only 0.1 m (Fig. 7 A). This is in contrast to observation point 2 where the maximum wave height reached 1.05 *m* within 15 min after the formation of the first tsunami waves off the east coast of Catania (Fig. 7 B and Table 6). Afterwards, the wave height tended to fall below 1 *m*. The wave heights at the 40th, 50th, 80th, 110th, 115th and 140th minutes were 0.8 *m*, 1.05 *m*, 0.25 *m*, 0.4 *m*, 0.25 *m*, 0.4 *m* and 0.25 *m*, respectively. At observation site 3, the maximum run-up height of 1.9 *m* occurred at the 17th minute (Fig. 7C and Table 6), then a second run-up wave of 1 *m* took place at the 40th minute. Subsequently, the wave height decreased to less than 1 *m*. However, at 83rd and 109th minutes, the wave height still stood at 0.9 and 0.8 *m* before finally declining to below 0.5 *m*. Observation points 4, 5 and 6 are negligible as the maximum run-up heights are only 0.5 *m*, 0.68 *m* and 0.06 *m*, accordingly (Fig. 7 D, E, and F). In Augusta and Syracuse the maximum run-up height was recorded at the 7th minute after tsunami wave generation (Fig. 8 A). Meanwhile, in Catania the maximum run-up height occurred at 17 min after the generation of the first phase of the tsunami (Fig. 8 B). The maximum run-up height and arrival time of tsunami waves at each observation location are shown in Table 6.

3.1.3. Scenario 3

Tsunami wave simulations based on the fault parameters of Gallais et al. [57] demonstrated that the estimated magnitude of the earthquake was M_w 6.61 (Fig. 9 and Table 7). At observation point 1, the maximum wave height was only 0.19 *m*, which can be said to not significantly threaten the safety of coastal residents (Fig. 10 A). At the second observation site, the maximum run-up height was 0.7 *m* at the 16th minute (Fig. 10 B). The wave heights at the 35th, 50th and 70th minutes were 0.42 *m*, 0.47 *m*, and 0.45 *m*, respectively. The simulated maximum run-up height that was higher compared to observation sites 1 and 2 was at observation site 3 which attained 0.9 *m* and took place after 15 min of tsunami generation (Fig. 10C). The waves in the following minutes were only around 0.5 *m*, especially 1 h after the first wave formed offshore. A significant wave height occurred at observation point 4 where the maximum run-up reached 1.8 *m* and it occurred in the 6th minute (Fig. 10 D). Then a tsunami backwash occurred which reduced the wave height to around 0.5 *m*. Even after the first 30 min of run-up, the wave height was only below 0.5 *m*. Meanwhile, the maximum run-up height of tsunami waves at observation location 5 was the same as the maximum height of tsunami waves at observation point 3 of 0.9 *m* which was recorded within 5 min after the first wave event (Fig. 10 E). The height of the second wave after the backwash of the first

Table 4
Maximum run-up height and arrival time of tsunami waves at the six observation sites based on earthquake-tsunami simulation scenario 1.

Location	Maximum run-up height (m)	Arrival time (minute)
STA 1	0.39	12
STA 2	1.75	12
STA 3	1.7	16
STA 4	4.4	7
STA 5	3.25	9
STA 6	0.68	15

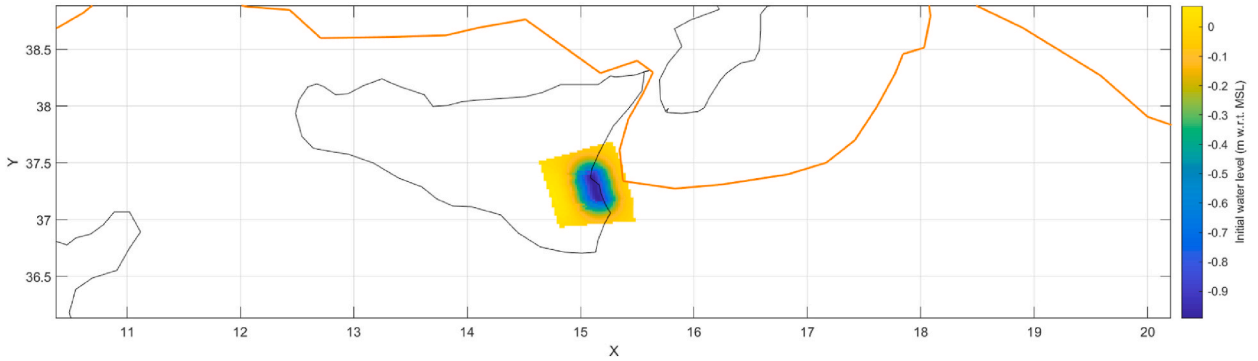

Fig. 6. The tsunamigenic source in scenario 2 is a fault movement with a length of 36 km and a slip of 5 *m*.

Table 5
Fault parameters and earthquake rupture in scenario 2. The magnitude of the earthquake triggered by fault displacement in scenario 2 is Mw 6.81 [4].

Fault parameter	Rupture input	Magnitude of earthquake (M_w)
Strike (°)	~N157E–N171E	6.81
Dip (°)	49	
Length (km)	36	
Width (km)	20.2	
Rake (°)	270	
Slip (m)	5	
Depth (km)	20	

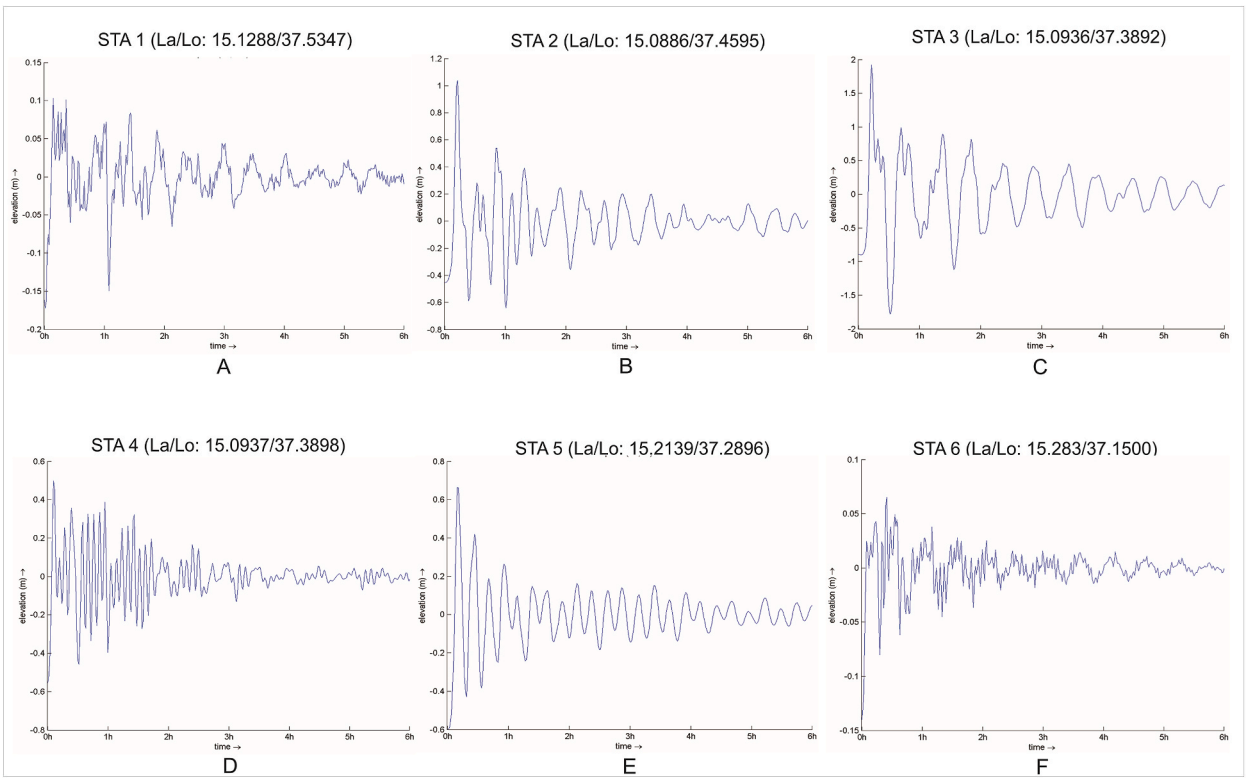

Fig. 7. The maximum run-up heights based on scenario 2 simulations at A. STA 1, B. STA 2, C. STA 3, D. STA 4, E. STA 5, and F. STA 6 are 0.1 *m*, 1.05 *m*, 1.9 *m*, 0.5 *m*, 0.68 *m*, and 0.06 *m*, respectively. The average tsunami inundation time lasted up to 1 h at STA 2 and 2 h at STA 3.

Table 6
Maximum run-up height and arrival time of tsunami wave propagation on the east coast of Sicily based on simulations of earthquake-tsunami scenario 2.

Location	Maximum run-up height (m)	Arrival time (minute)
STA 1	0.1	5
STA 2	1.05	15
STA 3	1.9	17
STA 4	0.5	7
STA 5	0.68	5
STA 6	0.06	25

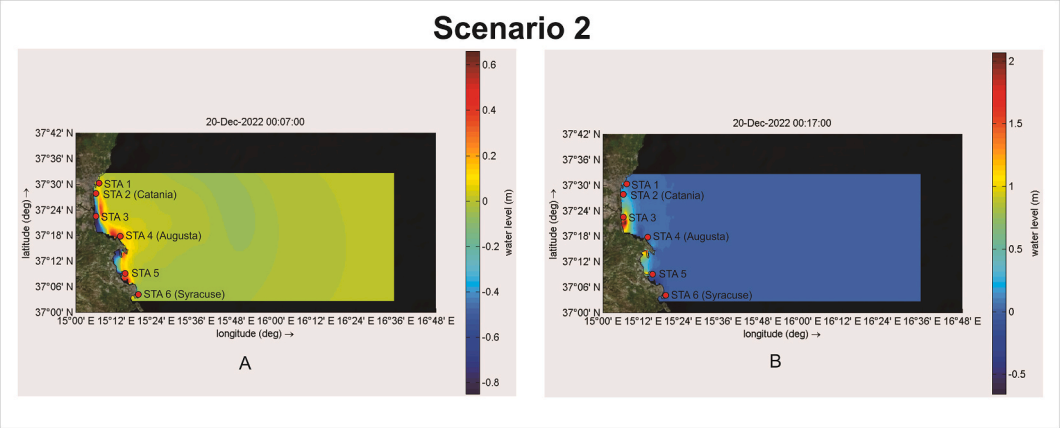

Fig. 8. A. The tsunami wave run-up at Augusta in the 7th minute was the highest level of the wave achieving 0.5 *m*. B. The highest peak of tsunami waves in Catania occurred in the 17th minute with a height of 1.9 *m*.

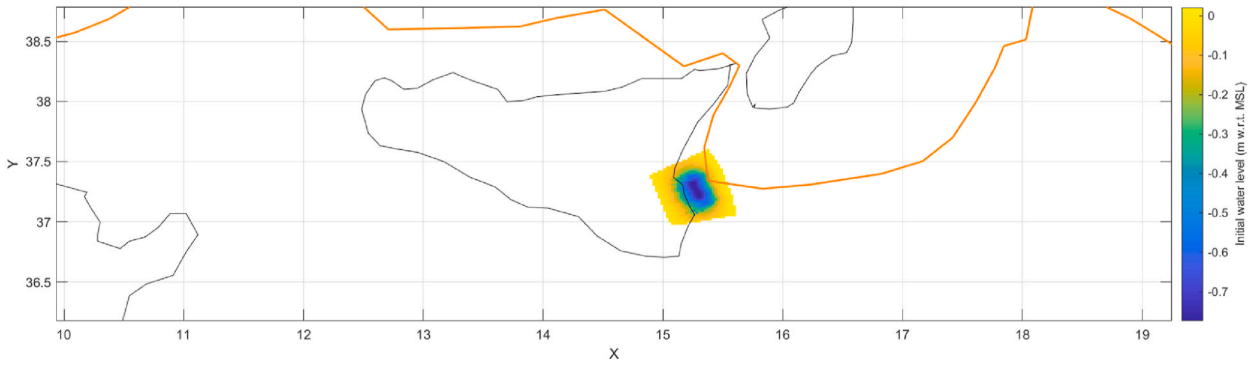

Fig. 9. The length, width, and slip of fault displacement in scenario 3 are 29 km, 16.7 km, and 5 *m* with NNW-SSE orientation.

Table 7
The fault and earthquake rupture parameters used in the tsunami simulation for scenario 3 are as follows. The magnitude of the earthquake in this scenario is Mw 6.61 [57].

Fault parameter	Rupture input	Magnitude of Earthquake (M_w)
Strike (°)	~N144E–N173E	6.61
Dip (°)	46	
Length (km)	29	
Width (km)	16.7	
Rake (°)	270	
Slip (m)	5	
Depth (km)	20	

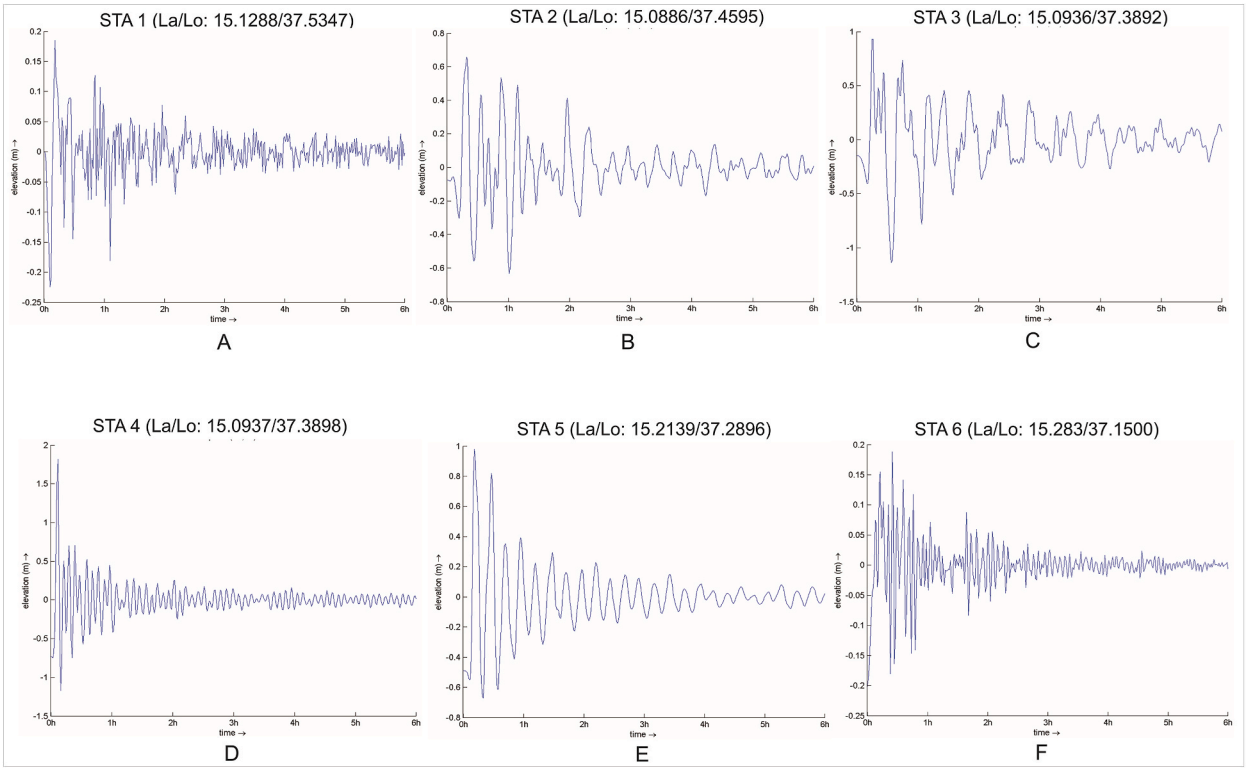

Fig. 10. The diagrams represent the tsunami wave's run-up height and propagation time from offshore to onshore for simulation scenario 3. The maximum sea water elevations at A. STA 1, B. STA 2, C. STA 3, D. STA 4, E. STA 5, and F. STA 6 are 0.19 *m*, 0.7 *m*, 0.9 *m*, 1.8 *m*, 0.9 *m*, and 0.19 *m*, respectively.

wave was only 0.4 *m* and it appeared in the 19th minute. Wave heights in the following minutes were between 0 and 0.2 *m*. At observation point 6 the wave height was less than 0.2 *m* and there was little chance of urban inundation (Fig. 10 F). Based on the tsunami simulations in Fig. 11 A and B, the maximum run-up heights in Augusta and Catania were reached at the 6th and 15th minutes after the generation of tsunami waves offshore. The estimated maximum run-up height and wave arrival time at all observation sites are provided in Table 8.

3.1.4. Scenario 4

The simulation results of the fault parameter of Gambino et al. [9] express that the predicted magnitude of the earthquake in 1693 was M_w 7.13 (Fig. 12 and Table 9). At observation site 1, the maximum run-up height reached 1.25 *m*, which occurred in the 12th

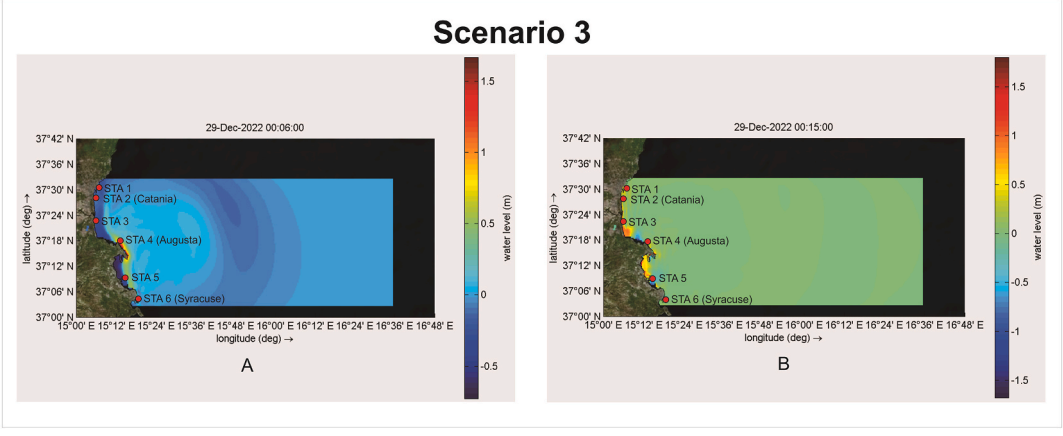

Fig. 11. Tsunami propagation modeling based on scenario 3 expresses that the maximum inundation in A. Augusta and B. Catania are 1.8 *m* and 0.9 *m* which occur at the 6th and 15th minute after the first wave generation offshore.

Table 8
The maximum run-up height, and tsunami wave arrival time at each observation site under scenario 3. At Augusta, which is also observation site 4, the maximum run-up height is more than 1.8 *m*.

Location	Maximum run-up height (m)	Arrival time (minute)
STA 1	0.19	5
STA 2	0.7	16
STA 3	0.9	15
STA 4	1.8	6
STA 5	0.9	5
STA 6	0.19	25

minute (Fig. 13 A). After that, the run-up height dropped below 1 *m*. It is likely that the inundation of seawater at this location took place within the 5th to the 90th minute after the generation of the first tsunami wave with an estimated height between 0.25 m and 0.75 *m*. At observation point 2, the maximum run-up height reached 5.9 *m* which occurred in the 15th minute after the generation of the first wave (Fig. 13 B). Even within 12–14 min, the wave height had reached 5.4 *m*. The subsequent wave heights in the 20th, 34th, 50th, and 80th minutes tended to decrease gradually by 3 *m*, 1.6 *m*, 1.5 *m*, and 0.9 *m*, respectively. After the 50th minute, the wave height was constant between 0 and 0.5 *m*. At observation site 3, the maximum wave height was 6.5 *m* and arrived at the 12th minute (Fig. 13C). At 35th minute a second wave arrived with a run-up height of about 2.5 *m* and then slowly decreased to 0–1 *m* in the following minutes. At observation site 4 in Augusta, the maximum run-up height of 4.2 *m* occurred in the 6th minute. Afterwards, the wave height decreased to 1 *m* and even less than 1 *m* from the 15th to the 90th minute after the first formation of tsunami waves (Fig. 13 D). At observation site 5 the maximum run-up height reached 7.7 m (Fig. 13 E), followed by a second run-up with a wave height of only 3.4 *m*. The tsunami inundation above 1 *m* lasted until the 50th minute and then gradually decreased until it returned to normal after the 90th minute. The first run-up waves at observation site 6 appeared at the 5th minute with a height of 1.75 m (Fig. 13 F), at the 13th minute the wave height was around 1.4 *m* and then descended below 1 *m* at the 15th minute onwards. It is expected that seawater saturated the area around observation site 6 for 80 min from the first run-up of the tsunami. Fig. 14 A, B, C, and D depict the time and height of maximum tsunami run-up at Syracuse, Augusta, the coast between Augusta and Syracuse (STA 5), and Catania (STA 2), respectively. The distribution of maximum run-up height and tsunami wave arrival time at each observation location is presented in Table 10.

3.1.5. Scenario 5

The magnitude of the earthquake estimated to have occurred off the east coast of Catania by applying the modified fault parameters of Okada [58,59] on Delft Dashboard was M_w 7.18 (Fig. 15 and Table 11). At the 12th minute at observation site 1, the tsunami run-up height reached its maximum point of 1.9 m (Fig. 16 A). At the 6th minute, the tsunami waves hit the shoreline with a height of 0.7 *m* and then rose significantly at the 12th minute. In the 15th minute, the wave height was still above 1 *m* but then dropped to below 1 *m*. The inundation of seawater around observation site 1 was predicted to continue for about 90 min. At observation site 2, the first phase run-up of tsunami waves began at the 10th minute with a height of 3.5 *m*. The maximum run-up height of 5.8 m was observed 6 min after the first phase of the run-up (Fig. 16 B). Subsequently, the wave height tended to fall to below 1 *m* by the 29th minute. Seawater still flooded the area around the observation site 2–90 min after the first wave generation period. At observation station 3, the first phase of tsunami waves reaching land has a height of up to 5.9 *m* and is the maximum point of run-up at this location. This first phase happened at the 13th minute after the formation of tsunami waves offshore (Fig. 16C). In the 15th minute, the wave height still stood at 5 *m* and then dropped in the following minutes to below 1 *m*. However, the second phase of run-up impacted observation site 3 in the 45th to 58th minutes with wave heights exceeding 2.5 *m* and then gradually descending to within 0–1 *m*. At observation site 4, the maximum run-up height was about 3 *m* which was experienced in the 7th minute (Fig. 16 D) and then declined to only 0–1 *m* after the 30th minute which is also assumed to be the second phase of run-up. About 40 min after the first run-up phase, the wave height was still

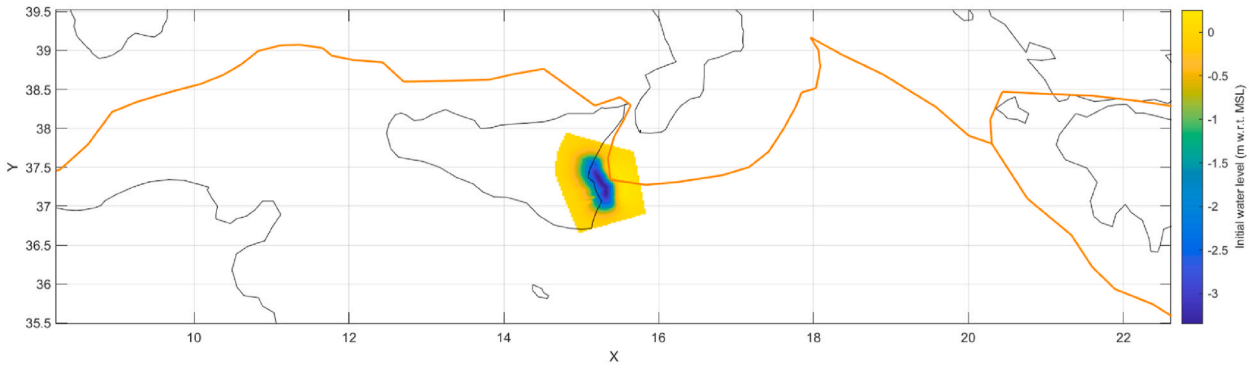

Fig. 12. The position of the fault displacement in scenario 4 extending from NNE to SSW along 58.5 km could cause an earthquake with a magnitude of M_w 7.13.

Table 9
Fault and earthquake rupture parameters utilized in tsunami simulation scenario 4. The slip length of the fault movement is 10 m [9].

Fault parameter	Rupture input	Magnitude of Earthquake (M_w)
Strike (°)	~N144E–N173E	7.13
Dip (°)	49	
Length (km)	58.5	
Width (km)	27.3	
Rake (°)	270	
Slip (m)	10	
Depth (km)	20	

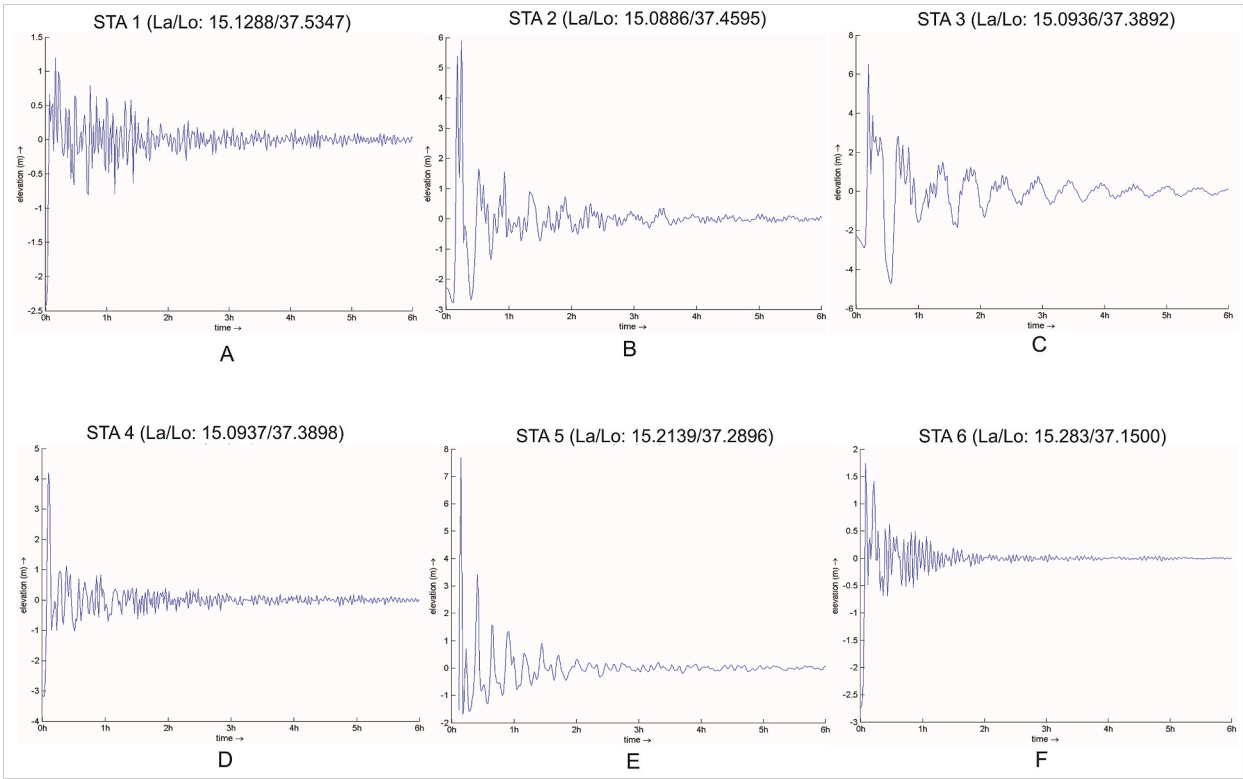

Fig. 13. The simulation graphs of tsunami wave run-up and propagation at A. STA 1, B. STA 2, C. STA 3, D. STA 4, E. STA 5, and F. STA 6 reveal that the inundation elevations at each of these observation locations are 1.25 *m*, 5.9 *m*, 6.5 *m*, 4.2 *m*, 7.7 *m*, and 1.75 *m*, correspondingly. The maximum sea water exposure time at each observation location is varied between one and 2 h.

between 0.5 m and 1 m. Seawater is forecast to still flood the coastal area up to 90 min after the initial run-up phase. At the 10th minute at observation location 5 the wave height attained 4.8 m and was the maximum run-up at this location (Fig. 16 E). Then the wave height was under 1 *m* after 50 min of maximum run-up. From the 70th to the 100th minute, the wave height was only around 0–1 *m* and this was the last time span of seawater inundation at this location. At the 9th minute, tsunami inundation took place at observation site 6 in Syracuse with a height of 1.7 *m* and this was also the maximum run-up height (Fig. 16 F). Five minutes following the maximum run-up phase the wave height was within 1.4 *m* and then fell continuously to below 0.5 *m* around the 20th to 30th minute. Beyond the 40th minute, the wave height was no longer significant and marked the end of the inundation of seawater on the coast around Syracuse. The simulated maximum run-up times and heights at Augusta (STA 4), Syracuse (STA 6), the area between Augusta and Syracuse (STA 5), and Catania (STA 2) are displayed in Fig. 17 A, B, C, and D. Meanwhile, the maximum run-up time and height of tsunami waves at each observation location are presented in Table 12.

3.1.6. Scenario 6

The simulated earthquake magnitude using the fault parameters of Monaco and Tortorici [11] was Mw 6.38 (Fig. 18 and Table 13). The maximum run-up height at observation site 1 was 0.125 *m* which was recorded at the 12th minute, then gradually reduced to 0–0.05 m (Fig. 19 A). The first run-up phase of the tsunami occurred at the 5th minute with a height of 0.075 *m*. The first run-up phase

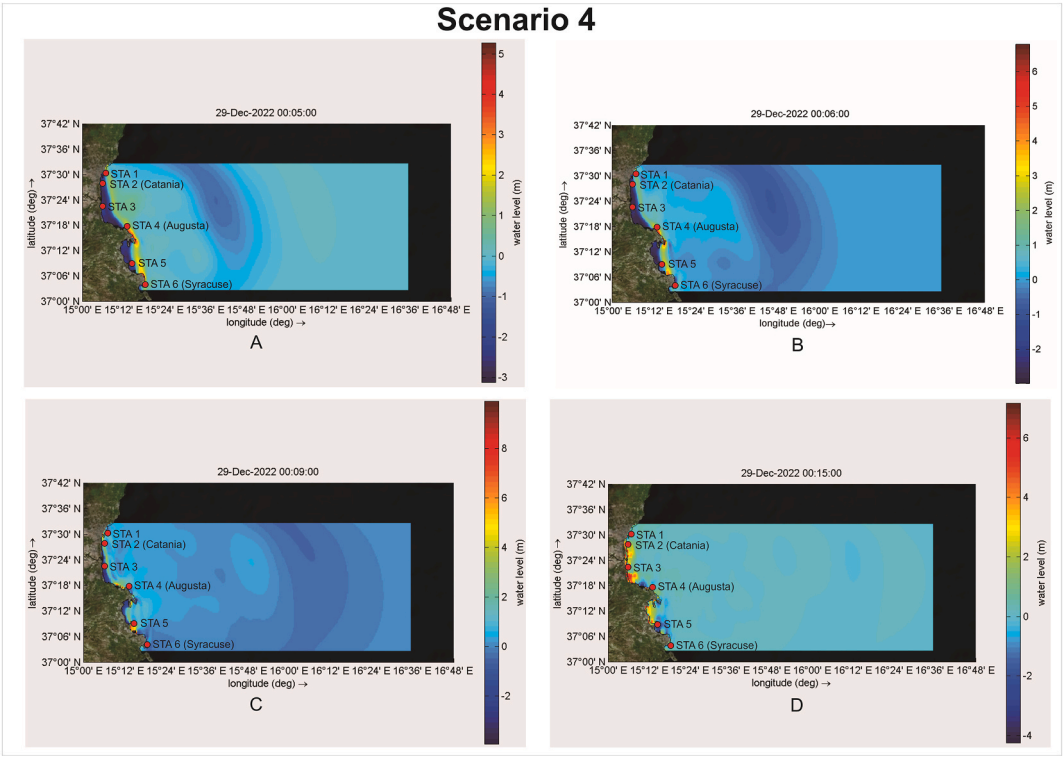

Fig. 14. A. Tsunami wave propagation at the 5th minute indicates that the run-up height of tsunami waves in Syracuse reached 1.75 *m*. B. At the 6th minute, the water level at STA 4 (Augusta) was estimated to be 4.2 *m*. C. The maximum water level of 7.7 *m* took place at STA 5 at the 9th minute. D. At the 15th minute, the tsunami run-up height at STA 2 (Catania) was 5.9 *m*.

Table 10
The maximum run-up height and arrival time of tsunami waves at each observation point were determined based on scenario 4. The run-up height at STA 5, located between Augusta and Syracuse, is the highest compared to other observation locations.

Location	Maximum run-up height (m)	Arrival time (minute)
STA 1	1.25	12
STA 2	5.9	15
STA 3	6.5	12
STA 4	4.2	6
STA 5	7.7	9
STA 6	1.75	5

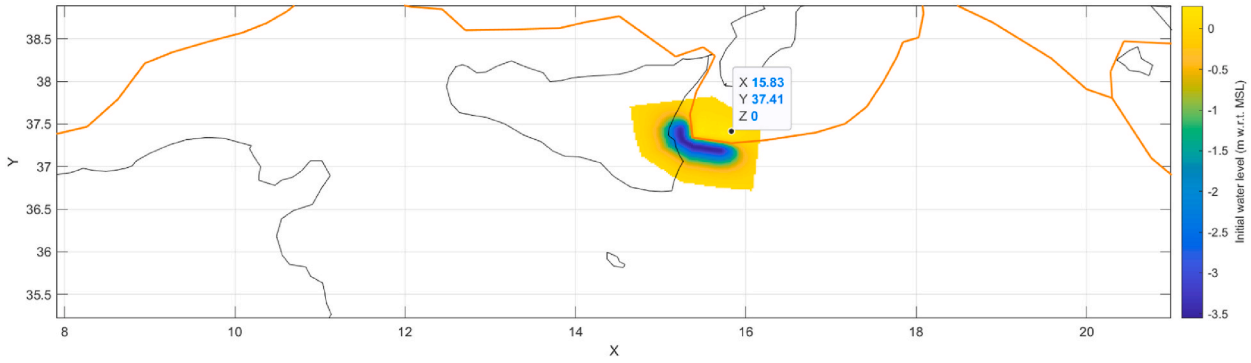

Fig. 15. The earthquake rupture that occurred in scenario 5 has two orientations, namely NNW–SSE and E–W, which are predicted to trigger a M_w 7.18 earthquake.

Table 11
The fault and earthquake rupture parameters applied in scenario 5. The length and width of fault movement are 62.1 km and 28.4 km, respectively [58,59].

Fault parameter	Rupture input	Magnitude of Earthquake (M_w)
Strike (°)	~N97E–N176E	7.18
Dip (°)	49	
Length (km)	62.1	
Width (km)	28.4	
Rake (°)	270	
Slip (m)	10	
Depth (km)	20	

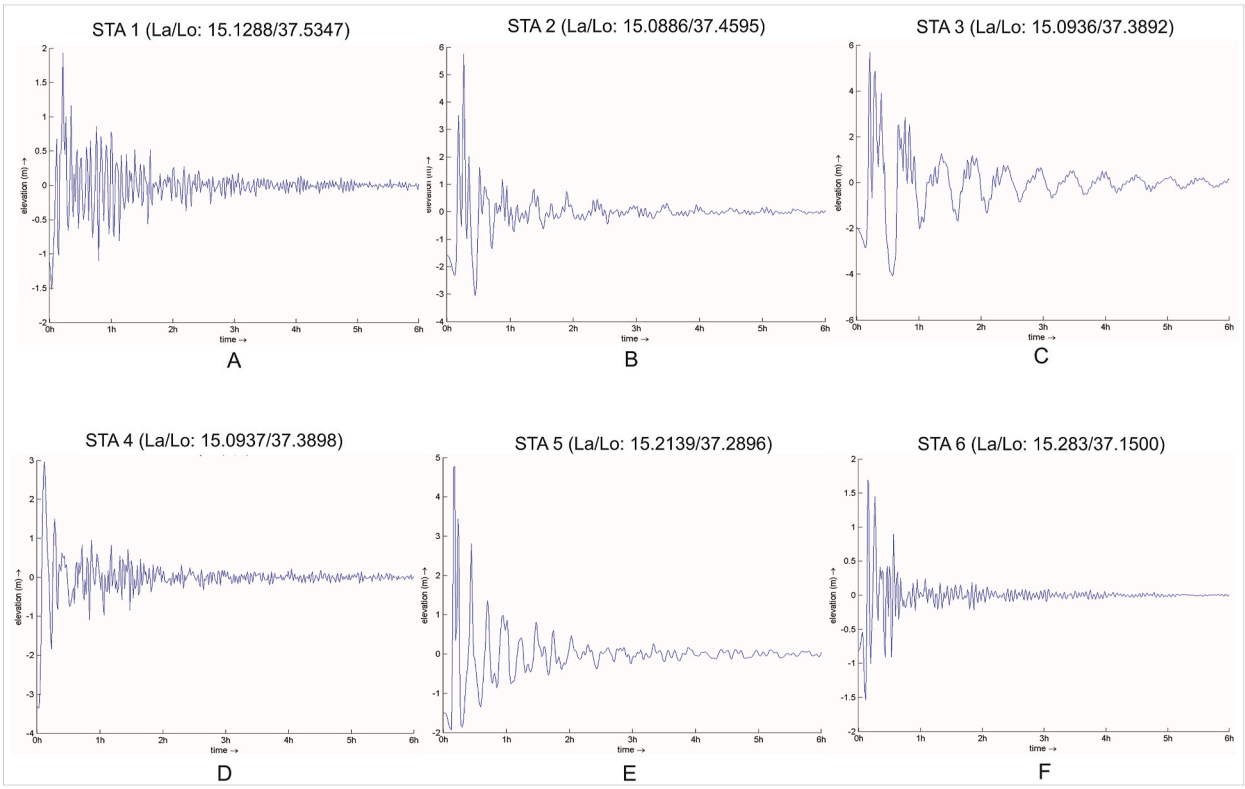

Fig. 16. The diagram of the relationship between run-up height and tsunami wave propagation according to simulation scenario 5 demonstrates that the crests of seawater flooding at A. STA 1, B. STA 2, C. STA 3, D. STA 4, E. STA 5, and F. STA 6 are 1.9 *m*, 5.8 *m*, 5.9 *m*, 3 *m*, 4.8 *m*, and 1.75 *m*, respectively. The duration of inundation in each of these observation locations is varied, ranging from 30 min to 2 h.

of the tsunami started in the 5th minute with a height of 0.075 *m*. The tsunami inundation at this location is expected to run for less than 30 min and might not generate notable wave heights inland. At the second observation location, the maximum run-up height was only 0.68 *m* or less than 1 *m*. This maximum height was reached in the 10th minute, which was the first run-up phase at this location (Fig. 19 B). At observation site 3, the maximum run-up height of the tsunami was also comparable to that of observation site 2, which was only 0.61 m (Fig. 19C). In the 40th to 50th minute, the tsunami height on land was expected to be only around 0.2–0.4 m and would not induce substantial inundation. Observation sites 4, 5, and 6 also exhibited the same phenomenon as observation sites 1, 2, and 3, i.e. the maximum run-up height was less than 1 *m*. At observation site 4 in Augusta the maximum wave height was 0.11 m (Fig. 19 D), at observation sites 5 and 6 around Syracuse the maximum run-up height was only 0.075 *m* and 0.019 *m*, correspondingly (Fig. 19 E and F). Since the overall inundation height was less than 0.5 *m*, it could be expected to have no considerable impact. The simulation of the maximum run-up time and height of tsunami waves at Catania, Augusta, and Syracuse are shown in Fig. 20 A, B, C, and D. The maximum run-up height and arrival time of tsunami waves at each observation location are presented in Table 14.

3.2. Tsunami inundation distance from catania coastline

The simulated maximum run-up height was utilized as one of the parameters, along with slope, elevation, and surface roughness, to

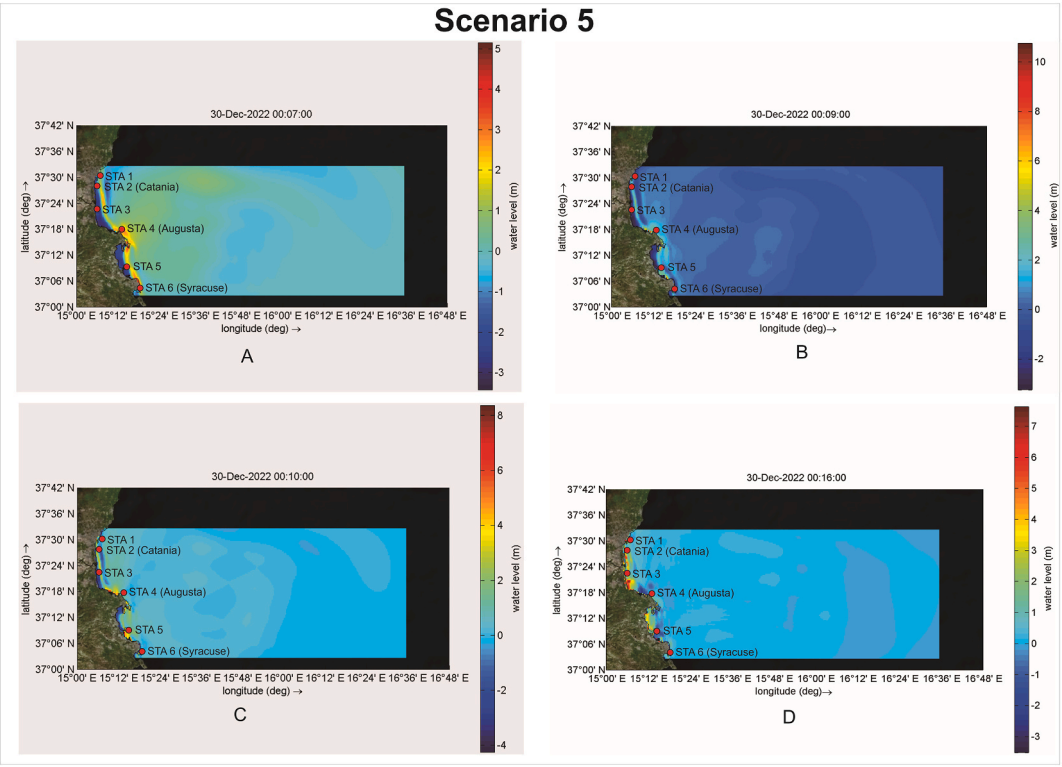

Fig. 17. A. At the 7th minute a maximum water level of 3 *m* occurred in Augusta. B. In Syracuse, the maximum water level of 1.7 *m* appeared at the 9th minute. C. The area between Augusta and Syracuse was inundated with 4.8 *m* of seawater at the 10th minute after tsunami wave generation. D. In Catania the maximum run-up height of 5.8 *m* was observed at the 16th minute.

Table 12
The maximum run-up height and arrival time of tsunami waves at each observation location according to scenario 5. The Catania region located at STA 2 and STA 3 recorded higher run-up heights compared to STA 4 (Augusta) and STA 6 (Syracuse).

Location	Maximum run-up height (m)	Arrival time (minute)
STA 1	1.9	12
STA 2	5.8	16
STA 3	5.9	13
STA 4	3	7
STA 5	4.8	10
STA 6	1.7	9

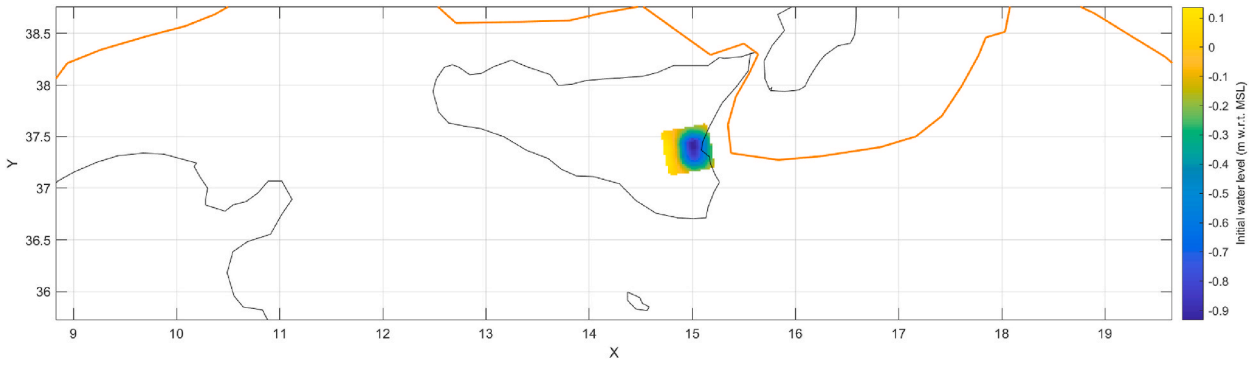

Fig. 18. The fault displacement location in scenario 6 is oriented NNE-SSW with a fault length and width of 21.2 km and 13.5 km, correspondingly.

Table 13
The fault parameters and earthquake rupture in scenario 6 may trigger an earthquake with a magnitude of Mw 6.38 [11].

Fault parameter	Rupture input	Magnitude of Earthquake (M_w)
Strike (°)	~N171E–N179E	6.38
Dip (°)	28	
Length (km)	21.2	
Width (km)	13.5	
Rake (°)	270	
Slip (m)	10	
Depth (km)	20	

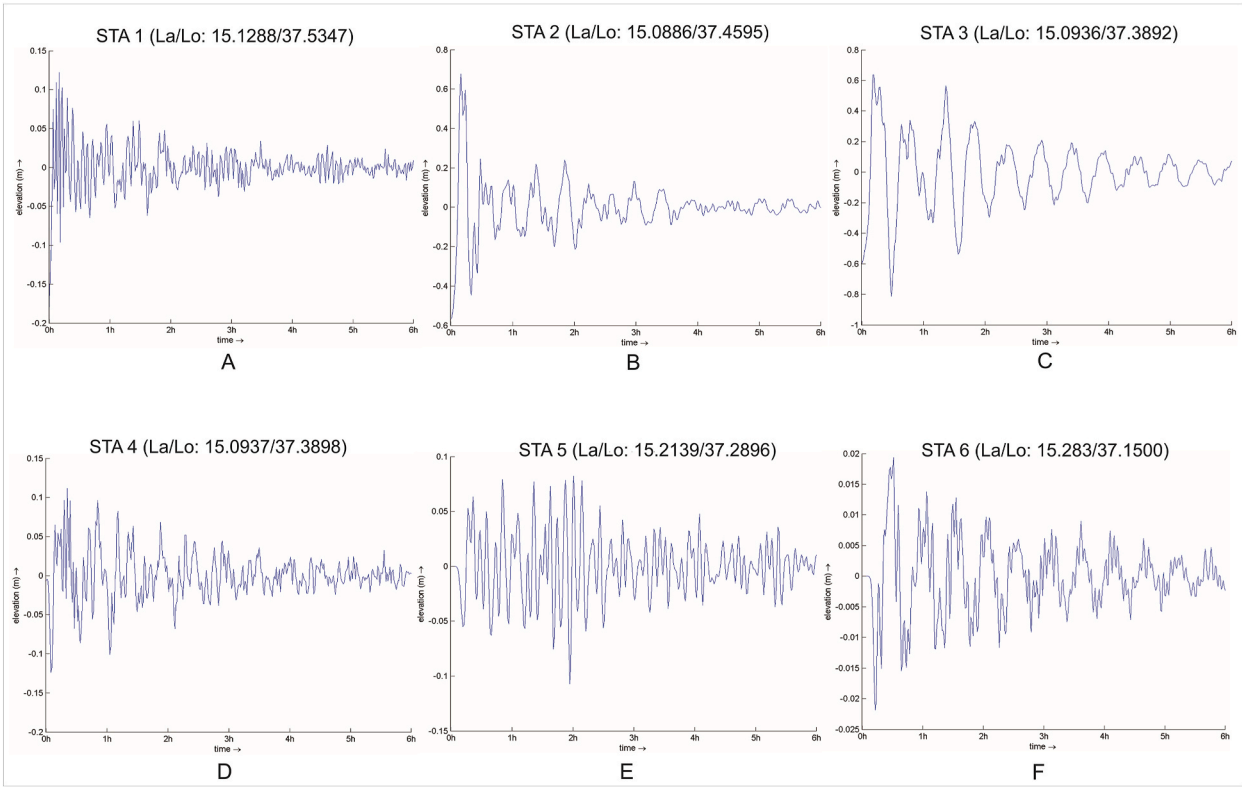

Fig. 19. The correlation curves between the elevation attained by tsunami waves and their propagation time reveal that at A. STA 1, B. STA 2, C. STA 3, D. STA 4, E. STA 5, and F. STA 6 the maximum elevations of inundated seawater are only 0.125 *m*, 0.68 *m*, 0.61 *m*, 0.11 *m*, 0.075 *m*, and 0.019 *m*, correspondingly. Meanwhile, the peak period for observation locations 1 to 3 is between minutes 10 to 12.

predict the furthest distance of tsunami inundation from the eastern coastline of Sicily. Based on the simulations of six scenarios, the furthest inundation distance in the Catania region is relatively shorter compared to that in the Augusta region (Fig. 21 A and B). In Catania, the seawater inundation distance from the coastline ranges from 32.5 *m* to 180 *m*, whereas in Augusta, the tsunami inundation distance reaches 8.5 *m*–318 *m*. The average inundation duration reaches 3600 s or 1 h. Scenario 4 represents the worst-case scenario, generating the highest run-up heights and longest inundation distances not only in Catania but also in Augusta. Conversely, scenario 6 is the lowest impact scenario, resulting in only 32.5 *m* inundation in Catania and 8.5 *m* in Augusta (as shown in Table 15), along with a maximum water level of 0.6 *m* in Catania and 0.11 *m* in Augusta.

3.3. Comparison between field evidence of tsunami deposits and simulation results

Based on the comparison of simulation results with evidence of tsunami deposits in the field [5,10,17,23], scenario 4 is the best model for describing the run-up height and inundation distance of tsunami deposits, especially in Augusta and Syracuse. In addition, the simulation of scenario 4 almost matches the description of the tsunami event found in the historical documents of Boccone [54] and Bottone [53]. There is a difference regarding the furthest inundation distance between these two historical documents and the results of this simulation (Fig. 22). According to both documents, the tsunami inundation distance was estimated to be 165 *m* inland in

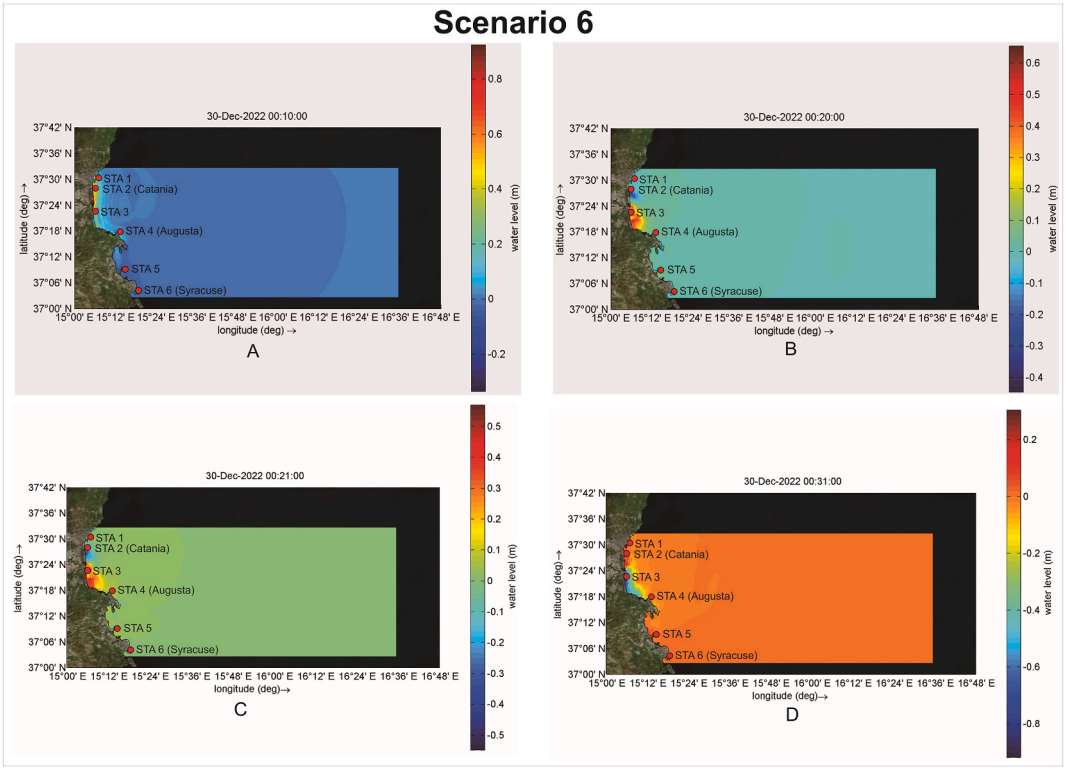

Fig. 20. A. The maximum run-up height of tsunami waves of 0.68 *m* in STA 2 (Catania) was observed in the 10th minute after the formation of the first wave offshore. B. At the 20th minute, the inundation height was still between 0.3 and 0.4 *m*, while in Augusta, STA 5, and Syracuse the wave height was negligible. C. At Augusta and STA 5 the maximum run-up height took place at the 21st minute after tsunami wave generation. D. At the 31st minute the run-up height at Syracuse was less than 0.2 *m*.

Table 14
The maximum run-up height for all observation locations under scenario 6 is below 1 *m*. In Catania (STA 2 and STA 3) the run-up height is higher than in Augusta (STA 4) or Syracuse (STA 6).

Location	Maximum run-up height (m)	Arrival time (minute)
STA 1	0.125	12
STA 2	0.68	10
STA 3	0.61	10
STA 4	0.11	21
STA 5	0.075	21
STA 6	0.019	30

Augusta City, but tsunami sediment evidence and simulations revealed that areas at a distance of 300–400 *m* from the shoreline were inundated with seawater. Meanwhile, the run-up heights between tsunami sediment evidence, simulation results, and historical documents exhibit similarities between 3 and 5 *m*. At STA 5, the simulation results indicate an overestimation of the run-up height of 7.7 *m*, while the prediction from tsunami sediment evidence in the field is only between 2 m and 4 m. The difference in interpretation is due to the different approaches used to analyze tsunami wave propagation on land. In the analysis of run-up heights based on evidence of tsunami deposits, the interpretation of tsunami wave run-up heights is based on the elevation of the location where tsunami deposits are found. However, it is possible that tsunami waves might attain higher elevations without leaving traces of the tsunami sediments. This is possible because the syn-depositional and post-depositional erosion processes of tsunami sediments are very intensive, thus tsunami sediment deposits during run-up could be eroded again by the tsunami waves during the backwash phase. Additionally, natural and anthropogenic processes also contributed to the removal of paleo-tsunami deposits. Moreover, coastal areas are highly dynamic. At STA 6 (Syracuse), the simulation provides a more detailed run-up height of 1.75 *m* compared to the results from the tsunami sediments which only estimate in the range of 1 m–2 m.

An illustration of the initial condition of the city of Catania before the tsunami and the moment of wave penetration further inland is presented in Figs. 23 and 24 A, B, C, D, E, and F while the process of inundation in Augusta and Syracuse is described in Figs. 25 and 26 A, B, C, D, and E. The statement and discovery of evidence of 1693 tsunami deposits by De Martini et al. [17] were reinforced by the discovery of similar deposits south of Syracuse characterized by dominant sand grain size with cross-bedding and clay lamination

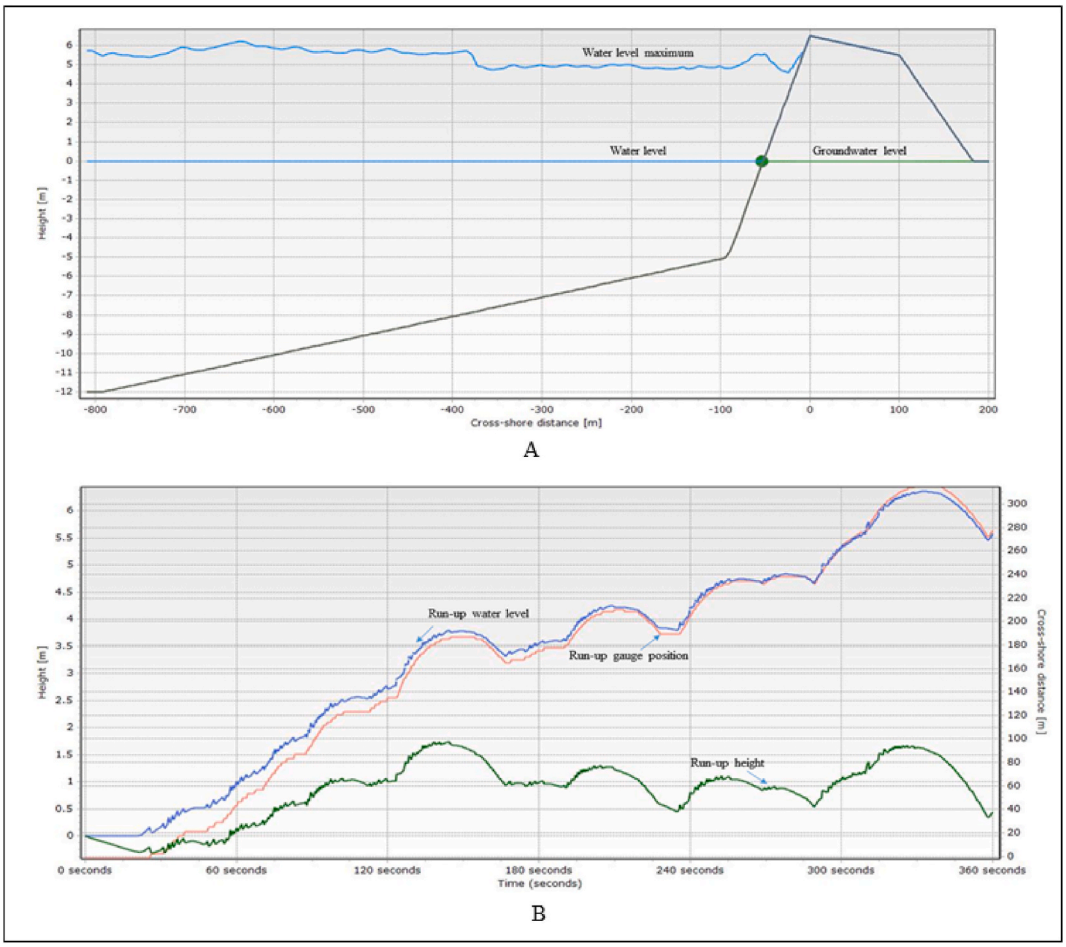

Fig. 21. A. The tsunami wave simulation by applying scenario 4 reveals that the maximum inundation distance in Catania is roughly 180 *m* from the current shoreline position. B. Inundation could extend up to 318 *m* from the shoreline between Augusta and Syracuse.

Table 15
The maximum tsunami inundation distance in Catania and Augusta. Based on scenario 4, the furthest inundation distance in Catania is 180 *m* while in Augusta it is up to 318 *m*.

Scenario	Inundation Distance in Catania	Inundation distance in Augusta
1	112.5 *m*	150 *m*
2	115 *m*	50 *m*
3	87.5 *m*	125 *m*
4	180 *m*	318 *m*
5	170 *m*	187.5 *m*
6	32.5 *m*	8.5 *m*

sedimentary structures. In south-eastern Sicily, there are also boulders weighing 182 t [10] that were most likely transported by water waves in the high energy regime.

3.4. Tsunami vulnerability index in Catania and Augusta

The analysis of tsunami hazard zones based on the Fuzzy membership method where the input parameters include the height and maximum inundation distance of waves from the Delft3D and XBeach simulation results can be depicted as shown in Fig. 27 A and B. Fuzzy membership values scale from 0 to 1, where if a classification value is approaching 1 then the area is more vulnerable to tsunamis, alternatively if the value of a class is close to 0 then the zone has a lower vulnerability. In this study, a value of 0.3–0.5 is included in the low vulnerability zone, 0.5–0.8 is classified as moderately vulnerable, and 0.8–1 is categorized as highly vulnerable. The red-colored zones represent a very high level of vulnerability to tsunami impacts. Meanwhile, the green colored zones express the

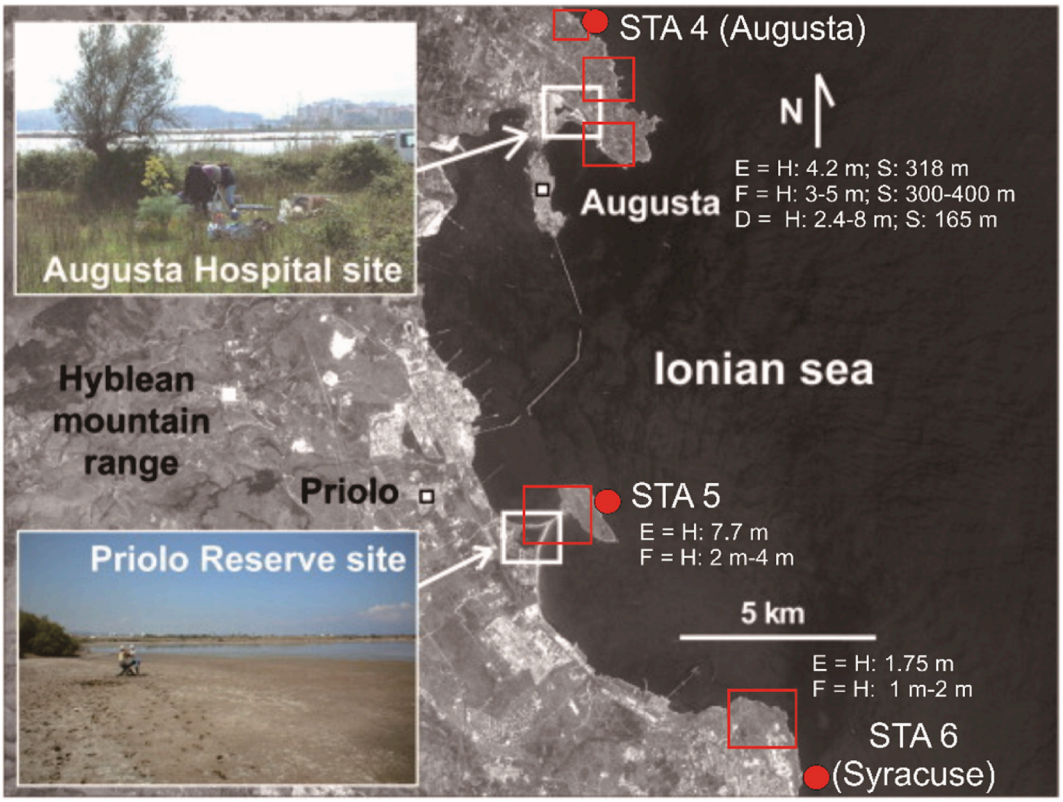

Fig. 22. The distribution of 1693 tsunami sediments in Augusta-Syracuse, historical documents, and simulation results of the worst-case scenario of the 1693 tsunami show consistency. Symbols E: simulation results; F: tsunami sediment analysis; D: tsunami historical documents; H: wave height; S: inundation distance [5,10,17,23,53,54].

areas with the lowest exposure if tsunami waves arrive and sweep the coastline. Tsunami wave propagation on land is mainly influenced by slope, land use, and the presence of rivers. The flatter the slope, the lower the vegetation density and the number of buildings as wave breakers, and the greater the number of water channels, the wider the penetration of the tsunami wave will be towards the land. Conversely, steep slopes, high densities of vegetation and breakwater structures, and the absence of rivers may prevent tsunami waves from propagating further inland.

4. Discussions

There have been several debates regarding the earthquake rupture that triggered the 1693 tsunami in Sicily. Prior to the tragic Mw 7.4 earthquake and tsunami on January 11, 1693, there was a seismic event at the same epicenter with a magnitude of Mw 6.2 on January 9, 1693, which did not generate a tsunami [56]. However, Argnani et al. [4] revised the magnitude of the January 11, 1693 earthquake from Mw 7.4 to Mw 7.2 based on seismic analysis of the Malta Escarpment in the Augusta-Syracuse segment. A smaller earthquake magnitude was suggested by the DISS Working Group [75], estimating it to be only Mw 6.6. Referring to the simulation results of earthquakes with Mw < 7, the tsunami run-up height on the east coast of Sicily would be less than 1 m, making it unlikely to inundate Augusta with over 100 m of sediment tsunami deposits found by De Martini et al. [17] and several boulders by Scicchitano et al. [10]. Another version was proposed by Monaco and Tortorici [11], stating that the magnitude of the January 11, 1693 earthquake was greater than Mw 7 because only earthquakes of that magnitude triggered tsunami waves above 1 m. Essentially, the geometry of the normal fault that caused the 1693 earthquake-tsunami is the same as the earthquake rupture geometries in 1783, 1905, and 1908, with a length between 30 km and 40 km. However, these statements were not accompanied by an analysis of slip length, rake, and fault displacement width. Furthermore, they did not estimate the run-up height and tsunami inundation range resulting from the implications of the earthquake. Deformation pattern predictions, including fault dimensions, slip, and seismotectonic implications, were conducted by Gambino et al. [9]. They argued that the strike, dip, length, width, rake, slip, and depth of fault displacement for the 1693 earthquake-tsunami were N144°E-N173°E, 49°, 58.5 km, 27.5 km, 270°, and 10 *m*, respectively. Scenario 4 simulations using these fault parameters triggered an earthquake with a magnitude of Mw 7.13.

Efforts to predict the magnitude of the 1693 earthquake have also been made by Scardino et al. [14], but the input slip parameter was only 5 m, not 10 m as suggested by Gambino et al. [9]. In that study, it was also mentioned that the run-up height of the tsunami wave was less than 1 m, with the inundation distance being less than 100 m from the Augusta coastline. However, De Martini et al. [5,

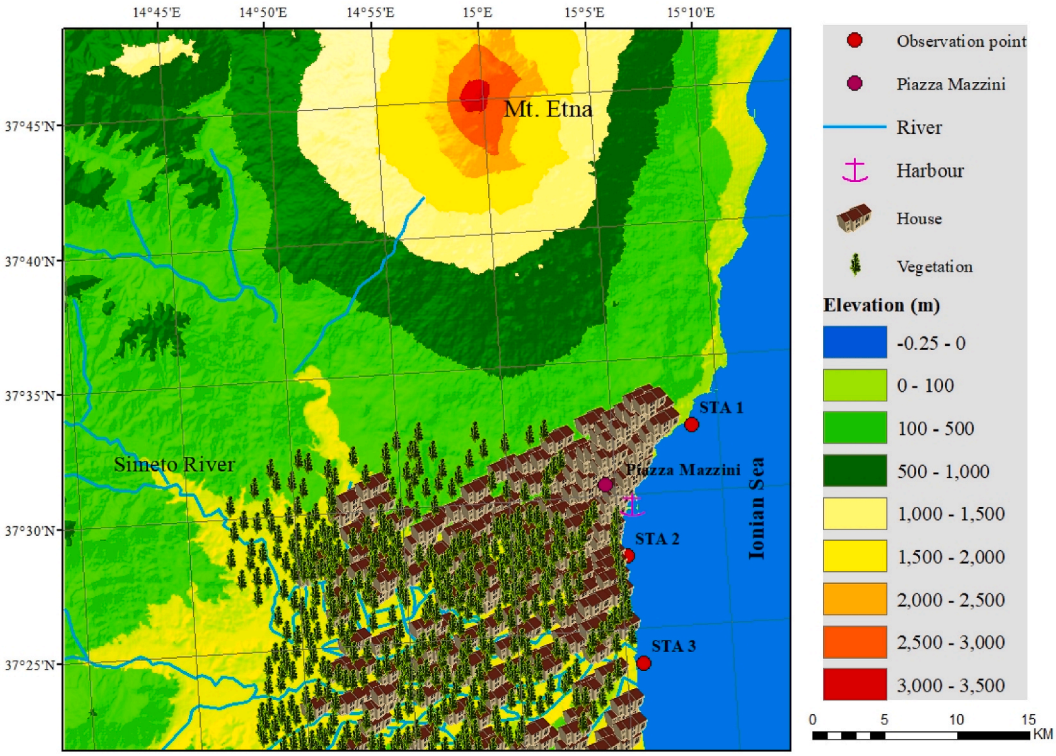

Fig. 23. Illustration of residential areas and public infrastructure in the northern sector of the Simeto River, Catania. The inundation of the 1693 tsunami is estimated to have covered Piazza Mazzini.

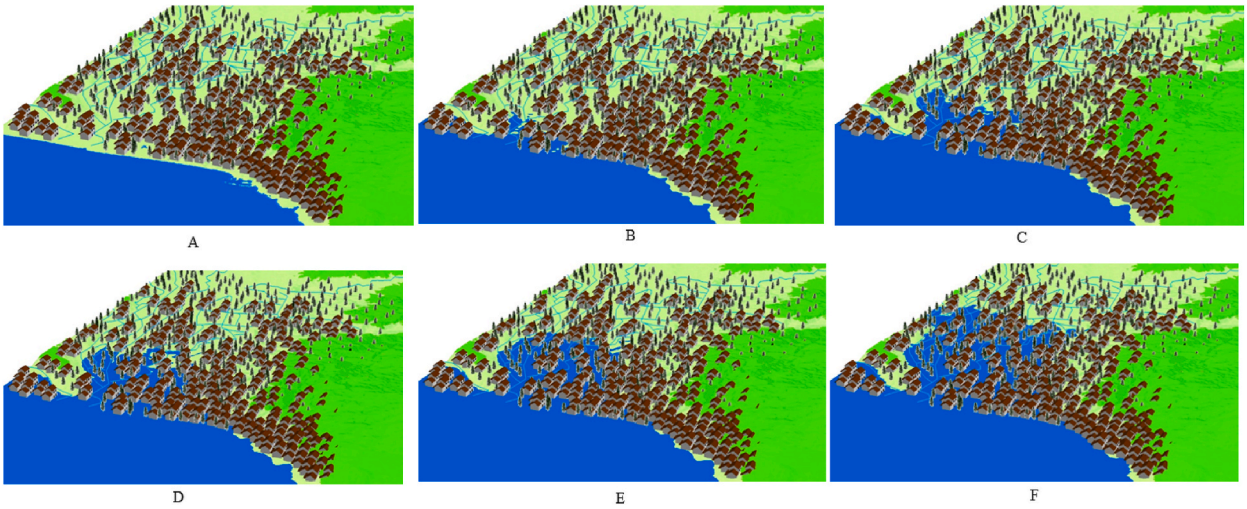

Fig. 24. An overview of the tsunami wave propagation upon arriving in Catania based on scenario 4. Figures A, B, C, and D depict the wave propagation from the 12th to the 34th minute after the initial wave generation offshore. On the other hand, Figures E and F illustrate the tsunami inundation resulting from the runoff of the second phase of run-up, which leads to the expansion of the inundation area.

17] discovered tsunami deposits at a distance of about 300 m from the coastline. However, De Martini et al. [5,17] did not find tsunami sediments in Catania, thus they could not predict the implications of this tsunami in the Catania area. Nevertheless, the discovery of several boulders by Scicchitano et al. [10] around Catania Beach indicates that the 1693 tsunami also affected the Catania region and could even transport and deposit boulders weighing 182 t. Additionally, historical documents by Boccone [54] and Bottone [53] also stated that the 1693 tsunami event caused seawater to inundate Piazza Mazzini, also known as San Filippo Square in Catania, which is currently located more than 100 m from the coastline. Both historical documents also described the tsunami wave in Augusta

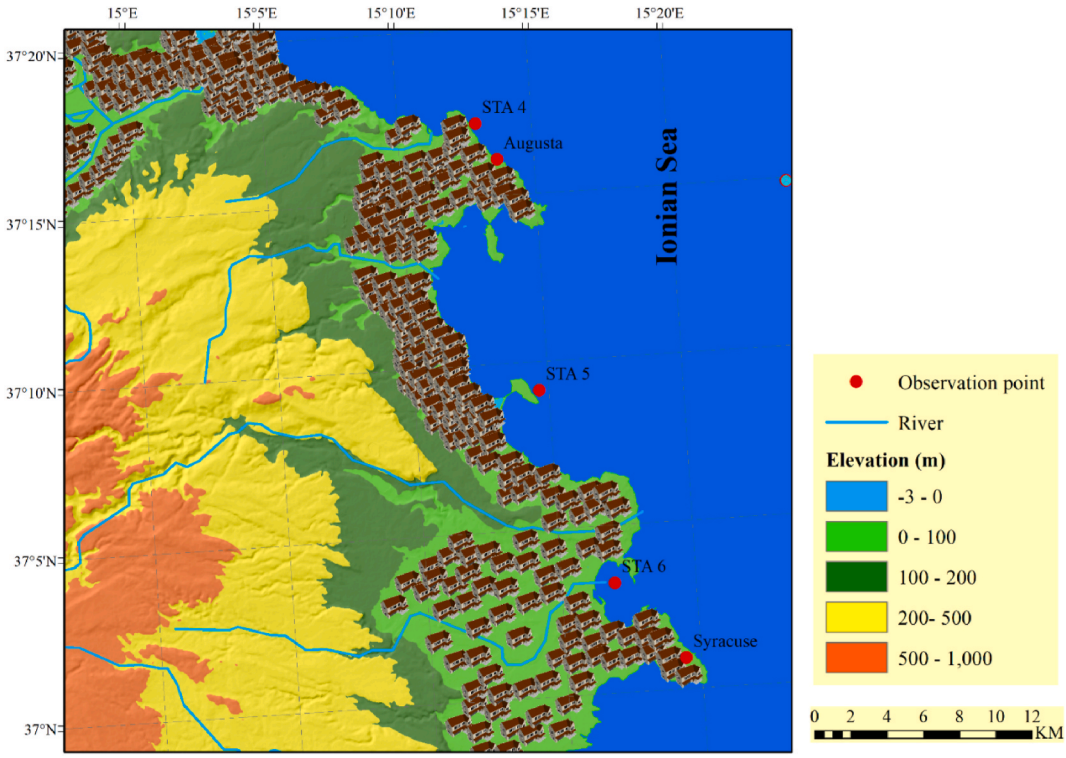

Fig. 25. A depiction of public facilities and residential housing in Augusta and Syracuse. This illustration represents the coastal conditions before the tsunami waves hit Augusta-Syracuse area.

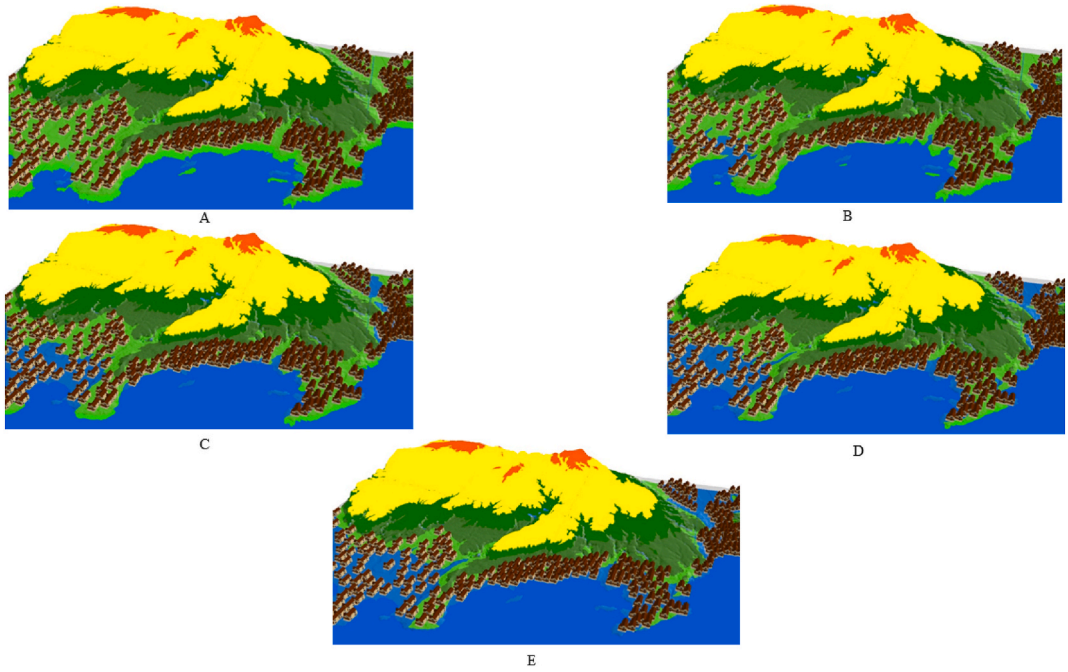

Fig. 26. The simulation of seawater inundation in Augusta and Syracuse based on scenario 4, estimated tsunami waves reached the mainland as far as 318 *m* from the STA 5 observation location. Each figure depicts the water level at minutes A. 5, B. 6, C. 7, D. 8, and E. 9.

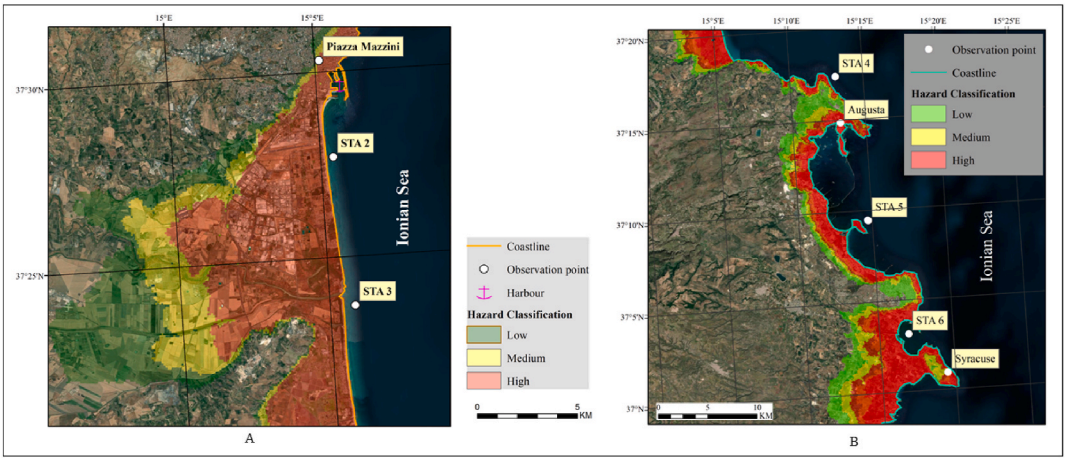

Fig. 27. A. Classification of tsunami hazard zones in Catania. B. Three tsunami hazard classes in Augusta-Syracuse from low to high vulnerability. The classification of tsunami vulnerability zones in Catania and Augusta-Syracuse is based on the Fuzzy membership method, where high vulnerability means expressing a Fuzzy membership value close to 1.

submerging the port area and San Domenico monastery up to a distance of approximately 165 m. In Syracuse, seawater also flooded the coastal area up to a distance of roughly 100–200 m from the coastline. Therefore, the deformation pattern and fault displacement parameters proposed by Gambino et al. [9] are the most suitable for illustrating the tsunamigenic source of 1693. A simulation using the fault geometry proposed by Okada [58,59] triggered a larger earthquake with a magnitude of Mw 7.18, but the run-up height and inundation distance of the tsunami in Catania, Augusta, and Syracuse were not as significant as the deformation pattern suggested by Gambino et al. [9]. This is because the fault orientation in Okada [58,59] changed from NNE-SSW to *E*-W in the Augusta region. Consequently, the main direction of tsunami wave propagation did not lead to eastern Sicily but rather to the southern Ionian Sea.

The landscape of Catania today and in 1693 is distinct, the sea level on the coast of Ognina, southeastern Sicily in that period was 0.25 *m* lower than today. The average sea level change in Catania according to NOAA [76] is an increase of 6.24 mm/year or equivalent to 2.05 ft/100 year. The uplift rate in Catania Plain according to Monaco et al. [77] is 0.56 mm/year. The erosion and accretion rates of the coastline south of the Simeto River, Catania are −1.646 *m*/year and 0.772 *m*/year while north of the Simeto River, Catania are −0.598 *m*/year and 1.334 *m*/year. Hence, if we refer to these data, the position of the coastline north of the Simeto River, Catania in 1693 was 242 *m* more advanced inland with an elevation of 1.85 *m* lower than today. Meanwhile, south of the Simeto River, Catania, the shoreline position in 1693 was 287 *m* more seaward with an elevation 1.85 *m* lower than today. The tsunamigenic source, according to the fault displacement parameters of Gambino et al. [9], triggers seawater inundation up to 180 m in the Catania-Augusta area and 318 m in the Augusta-Syracuse area. The maximum estimated run-up height reaches 6.5 m in the city of Catania, with an arrival time of 12 min after the tsunami generation at the tsunamigenic source. Meanwhile, the maximum run-up height and arrival time of the tsunami wave in Augusta-Syracuse are 7.7 m and 9 min, respectively. The port areas of Catania and Augusta fall into the red zone or high vulnerability zone. In Catania, the Catania International Airport area and San Filippo Square are categorized as high risk vulnerability zones. Meanwhile, in Augusta and Syracuse, the areas classified as the most prone to tsunami impacts, in addition to the ports, include Monte Tauro Cape, Augusta Bay, Magnisi Peninsula, and Santa Panagia Cape, which are tourist destinations in Sicily.

Tsunami wave propagation is relatively more rapid in areas close to rivers, gentle slopes, and low elevations. Settlements situated in locations with these characteristics are more vulnerable to impact compared to settlements distant from rivers, steep slopes, and high elevations [78]. Settlements and other buildings located near the coastline would be more significantly affected than those located far from the coastline. This is mainly because the height of the tsunami waves upon reaching the coastline is higher than the waves that have propagated far inland [78]. Moreover, the transportation energy and wave flow rates are robust and rapid, potentially damaging buildings and stranding people more substantially. Other factors that influence tsunami vulnerability are surface roughness and distance from the earthquake source [62,79]. Areas that have high surface roughness and proximity to tsunamigenic sources are more likely to be vulnerable to the devastating consequences of tsunamis [62,78]. Surface roughness is related to the land use of an area; the presence of breakwater structures and a high density of vegetation could reduce the energy and flow rate of tsunami waves [80].

5. Conclusions

The debate regarding the run-up height, inundation distance, and arrival time of the 1693 tsunami waves in eastern Sicily has been resolved through multi-scenario simulations that integrate earthquake rupture parameters, tsunami sediment evidence, and historical documents describing the tsunami event. We conclude that the 1693 tsunami simulation based on the earthquake rupture parameters proposed by Gambino et al. [9] is an accurate model for describing the penetration of tsunami waves along the eastern coast of Sicily. As a result of this tsunami event, the Catania-Augusta area is predicted to be inundated by seawater up to 6.5 m, with the tsunami wave penetrating inland for a distance of 180 m and arriving 12 min after the initial generation at the earthquake source. Meanwhile, along

the Augusta-Syracuse stretch, the maximum run-up height reaches 7.7 m, with a maximum inundation distance and arrival time of 318 m and 9 min, respectively. These scenarios align with the discovery of tsunami sediments at a distance of approximately 300 m from the Augusta coastline and the historical documents by Boccone [54] and Bottone [53] mentioning the submersion of the harbor and the San Domenico monastery. Another important finding and contribution is the mapping of tsunami-prone areas along the Catania-Syracuse coastline, which has not been previously addressed in research. This study reveals that in Catania, the harbor area, the airport, and even San Filippo Square are classified as high vulnerability zones. Meanwhile, the most tsunami-prone zones in Augusta and Syracuse include Monte Tauro Cape, Augusta Bay, Magnisi Peninsula, and Santa Panagia Cape. These findings could be used as a reference to search for the presence of paleotsunami deposits in Catania, which have not been discovered to date, and might be utilized by stakeholders to enhance tsunami disaster mitigation programs, especially along the eastern coast of Sicily. The integration of multi-scenario simulation methods with tsunami sediment evidence could be employed in various tsunami case studies to obtain more accurate results regarding the illustration of paleotsunami wave propagation.

Author contribution statement

FX Anjar Tri Laksono: Conceived and designed the experiments; Performed the experiments; Analyzed and interpreted the data; Contributed reagents, materials, analysis tools or data; Wrote the paper.

Data availability statement

Data will be made available on request.

Funding

The research was funded by UNKP program with research grant number ÚNKP-22-3-I-PTE-1403 for 2022/2023 and University of Pécs.

Declaration of competing interest

The authors declare that they have no known competing financial interests or personal relationships that could have appeared to influence the work reported in this paper.

References

[1] A. Polonia, L. Torelli, A. Artoni, M. Carlini, C. Faccenna, L. Ferranti, L. Gasperini, R. Govers, D. Klaeschen, C. Monaco, G. Neri, N. Nijholt, B. Orecchio, R. Wortel, The Ionian and Alfeo-Etna fault zones: new segments of an evolving plate boundary in the central Mediterranean Sea? Tectonophysics 675 (2016) 69–90, https://doi.org/10.1016/j.tecto.2016.03.016.
[2] M.A. Gutscher, S. Dominguez, B.M. de Lepinay, L. Pinheiro, F. Gallais, N. Babonneau, A. Cattaneo, Y.L. Faou, G. Barreca, A. Micallef, M. Rovere, Tectonic expression of an active slab tear from high-resolution seismic and bathymetric data offshore Sicily (Ionian Sea), Tectonics 35 (2016) 39–54, https://doi.org/10.1002/2015TC003898.
[3] A. Smedile, P.M. De Martini, D. Pantosti, L. Bellucci, P. Del Carlo, L. Gasperini, C. Pirrotta, A. Polonia, E. Boschi, Possible tsunami signatures from an integrated study in the Augusta Bay offshore (Eastern Sicily-Italy), Mar. Geol. 281 (2011) 1–13, https://doi.org/10.1016/j.margeo.2011.01.002.
[4] A. Argnani, A. Armigliato, G. Pagnoni, F. Zaniboni, S. Tinti, C. Bonazzi, Active tectonics along the submarine slope of south-eastern Sicily and the source of the 11 January 1693 earthquake and tsunami, Nat. Hazards Earth Syst. Sci. 12 (2012) 1311–1319, https://doi.org/10.5194/nhess-12-1311-2012.
[5] P.M. De Martini, M.S. Barbano, D. Pantosti, A. Smedile, C. Pirrotta, P. Del Carlo, S. Pinzi, Geological evidence for paleotsunamis along eastern Sicily (Italy): an overview, Nat. Hazards Earth Syst. Sci. 12 (2012) 2569–2580, https://doi.org/10.5194/nhess-12-2569-2012.
[6] G. Scicchitano, S. Gambino, G. Scardino, G. Barreca, F. Gross, G. Mastronuzzi, C. Monaco, The enigmatic 1693 AD tsunami in the eastern Mediterranean Sea: new insights on the triggering mechanisms and propagation dynamics, Sci. Rep. 12 (2022) 9573, https://doi.org/10.1038/s41598-022-13538-x.
[7] Tinti, S., Maramai, A., Graziani, L. The new catalogue of Italian Tsunamis. Nat. Hazards 33, 439-465. https://doi.org/10.1023/B:NHAZ.0000048469.51059.65.
[8] A. Smedile, F. Molisso, C. Chagúe, M. Iorio, P.M. De Martini, S. Pinzi, P.E.F. Collins, L. Sagnotti, D. Pantosti, New coring study in Augusta Bay expands understanding of offshore tsunami deposits (Eastern Sicily, Italy), Sedimentology 67 (2020) 1553–1576, https://doi.org/10.1111/sed.12581.
[9] S. Gambino, G. Barreca, F. Gross, C. Monaco, S. Krastel, M.A. Gutscher, Deformation pattern of the northern sector of the Malta escarpment (Offshore SE Sicily, Italy): fault dimension, slip prediction, and seismotectonic implications, Front. Earth Sci. 8 (2021), 594176, https://doi.org/10.3389/feart.2020.594176.
[10] G. Scicchitano, C. Monaco, L. Tortorici, Large boulder deposits by tsunami waves along the Ionian coast of south-eastern Sicily (Italy), Mar. Geol. 238 (2007) 75–91, https://doi.org/10.1016/j.margeo.2006.12.005.
[11] C. Monaco, L. Tortorici, Active faulting and related tsunamis in eastern Sicily and south-western Calabria, Boll. di Geofis. Teor. ed Appl. 48 (2007) 163–184.
[12] R. Azzaro, M.S. Barbano, A. Moroni, M. Mucciarelli, M. Stucchi, The seismic history of Catania, J. Seismol. 3 (1999) 235–252, https://doi.org/10.1023/A:1009818313629.
[13] A. Smedile, P.M. De Martini, D. Pantosti, Combining inland and offshore paleotsunamis evidence: the Augusta Bay (eastern Sicily, Italy) case study, Nat. Hazards Earth Syst. Sci. 12 (2012) 2557–2567, https://doi.org/10.5194/nhess-12-2557-2012.
[14] G. Scardino, A. Rizzo, V. De Santis, D. Kyriakoudi, A. Rovere, M. Vacchi, S. Torrisi, G. Scicchitano, Insights on the origin of multiple tsunami events affected the archaeological site of Ognina (south-eastern Sicily, Italy), Quat. Int. 638 (2021) 122–139, https://doi.org/10.1016/j.quaint.2021.09.013.
[15] E. Guidoboni, A. Comastri, G. Traina, Catalogue of Ancient Earthquakes in the Mediterranean Area up to the 10th Century, fifty-fifth ed., Istituto nazionale di geofisica, Rome, 1994.
[16] A. Rovida, M. Locati, R. Camassi, B. Lolli, P. Gasperini, The Italian earthquake catalogue CPTI15, Bull. Earthq. Eng. 18 (2020) 2953–2984, https://doi.org/10.1007/s10518-020-00818-y.
[17] P.M. De Martini, M.S. Barbano, A. Smedile, F. Gerardi, D. Pantosti, P. Del Carlo, C. Pirrota, A unique 4000 year long geological record of multiple tsunami inundations in the Augusta Bay (eastern Sicily, Italy), Mar. Geol. 276 (2010) 42–57, https://doi.org/10.1016/j.margeo.2010.07.005.
[18] G. Scicchitano, F. Antonioli, E.F.C. Berlinghieri, A. Dutton, C. Monaco, Submerged archaeological sites along the Ionian coast of southeastern Sicily (Italy) and implications for the Holocene relative sea-level change, Quat. Res. 70 (2008) 26–39, https://doi.org/10.1016/j.yqres.2008.03.008.

[19] C. Lo Re, G. Manno, M. Basile, M.F. Ferrotto, L. Cavaleri, G. Ciraolo, Tsunami vulnerability evaluation for a small ancient village on eastern sicily coast, J. Mar. Sci. Eng. 10 (2022) 268, https://doi.org/10.3390/jmse10020268.

[20] A. Piatanesi, S. Tinti, A revision of the 1693 eastern Sicily earthquake and tsunami, J. Geophys. Res. Solid Earth 103 (1998) 2749–2758, https://doi.org/10.1029/97JB03403.

[21] S.J. Gibbons, S. Lorito, J. Macias, F. Løvholt, J. Selva, M. Volpe, C.S. Linares, A. Babeyko, B. Brizuela, A. Cirella, M.J. Castro, M. de la Asuncion, P. Lanucara, S. Glimsdal, M.C. Lorenzino, M. Nazaria, L. Pizzimenti, F. Romano, A. Scala, R. Tonini, J.M.G. Vida, M. Vöge, Probabilistic tsunami hazard analysis: high performance computing for massive scale inundation simulations, Front. Earth Sci. 8 (2020), 591549, https://doi.org/10.3389/feart.2020.591549.

[22] R. Tonini, A. Armigliato, G. Pagnoni, F. Zaniboni, S. Tinti, Tsunami hazard for the city of Catania, eastern sicily, Italy, assessed by means of worst-case credible tsunami scenario analysis (WCTSA), Nat. Hazards Earth Syst. Sci. 11 (2011) 1217–1232, https://doi.org/10.5194/nhess-11-1217-2011.

[23] M.S. Barbano, C. Pirrotta, F. Gerardi, Large boulders along the south-eastern Ionian coast of Sicily: storm or tsunami deposits? Mar. Geol. 275 (2010) 140–154, https://doi.org/10.1016/j.margeo.2010.05.005.

[24] G. Piazza, Squatting social centres in a Sicilian city: liberated spaces and urban protest actors, Antipode 50 (2018) 498–522, https://doi.org/10.1111/anti.12286.

[25] E. Boschi, E. Guidoboni, G. Ferrari, D. Mariotti, G. Valensise, P. Gasperini, Catalogue of strong Italian earthquakes from 461 B.C. To 1997, in: Italian), fourth ed., Compositori, Bologna, 2000.

[26] M. Rebesco, A. Camerlenghi, V. Munari, R. Monsetti, J. Ford, A. Micallef, L. Facchin, Bottom current-controlled quaternary sedimentation at the foot of the Malta escarpment (Ionian Basin, mediterranean), Mar. Geol. 441 (2021), 106596, https://doi.org/10.1016/j.margeo.2021.106596.

[27] A. Billi, L. Minelli, B. Orecchio, D. Presti, Constraints to the cause of three historical tsunamis (1908, 1783, and 1693) in the Messina straits region, Sicily, southern Italy, Seismol Res. Lett. 81 (2010) 907–915, https://doi.org/10.1785/gssrl.81.6.907.

[28] A. Micallef, A. Georgiopoulou, J. Mountjoy, V.A.I. Huvenne, C.L. Iacono, T.L. Bas, P.D. Carlo, D.C. Otero, Outer shelf seafloor geomorphology along a carbonate escarpment: the eastern Malta Plateau, Mediterranean Sea, Continent. Shelf Res. 131 (2016) 12–27, https://doi.org/10.1016/j.csr.2016.11.002.

[29] R. Scandone, Models of volcanic processes: a review and some new ideas, Bull. Volcanol. 44 (1981) 256–267, https://doi.org/10.1007/BF02600563.

[30] A.M.C. Şengör, Mid-mesozoic closure of permo-triassic tethys and its implications, Nature 279 (1979) 590–593, https://doi.org/10.1038/279590a0.

[31] Z. Ben-Avraham, M. Grasso, Crustal structure variations and transcurrent faulting at the eastern and western margins of the eastern Mediterranean, Tectonophysics 196 (1991) 269–277, https://doi.org/10.1016/0040-1951(91)90326-N.

[32] R. Catalano, C. Doglioni, S. Merlini, On the mesozoic Ionian Basin, Geophys. J. Int. 144 (2001) 49–64, https://doi.org/10.1046/j.0956-540X.2000.01287.x.

[33] F. Gallais, M.A. Gutscher, D. Graindorge, N. Chamot-Rooke, D. Klaeschen, A Miocene tectonic inversion in the Ionian Sea (central Mediterranean): evidence from multichannel seismic data, J. Geophys. Res. Solid Earth 116 (2011) B12, https://doi.org/10.1029/2011JB008505.

[34] A. Micallef, A. Camerlenghi, A. Georgiopoulou, D.G. Castellanos, M.A. Gutscher, C.L. Iacono, V.A.I. Huvenne, J.J. Mountjoy, C.K. Paull, T.L. Bas, D. Spatola, L. Facchin, D. Accettella, Geomorphic evolution of the Malta Escarpment and implications for the Messinian evaporative drawdown in the eastern Mediterranean Sea, Geomorphology 327 (2019) 264–283, https://doi.org/10.1016/j.geomorph.2018.11.012.

[35] M. Meschis, G. Scicchitano, G.P. Roberts, J. Robertson, G. Barreca, C. Monaco, C. Spampinato, D. Sahy, F. Antonioli, Z.K. Mildon, G. Scardino, Regional deformation and offshore crustal local faulting as combined processes to explain uplift through time constrained by investigating differentially uplifted late quaternary paleoshorelines: the foreland Hyblean Plateau, SE sicily, Tectonics 39 (2020), e2020TC006187, https://doi.org/10.1029/2020TC006187.

[36] C.R. Spampinato, B. Costa, A. Di Stefano, C. Monaco, G. Scicchitano, The contribution of tectonics to relative sea-level change during the Holocene in coastal south-eastern Sicily: new data from boreholes, Quat. Int. 232 (2011) 214–227, https://doi.org/10.1016/j.quaint.2010.06.025.

[37] C.R. Spampinato, G. Scicchitano, L. Ferranti, C. Monaco, Raised Holocene paleo-shorelines along the Capo Schisò coast, Taormina: new evidence of recent co-seismic deformation in northeastern Sicily (Italy), J. Geodyn. 55 (2012) 18–31, https://doi.org/10.1016/j.jog.2011.11.007.

[38] G. Scicchitano, B. Costa, A. Di Stefano, S.G. Longhitano, C. Monaco, Tsunami and storm deposits preserved within a ria-type rocky coastal setting (Siracusa, SE Sicily), Zeitschrift fur Geomorphol 54 (2010) 51–77, https://doi.org/10.1127/0372-8854/2010/0054S3-0019.

[39] D. Dellong, F. Klingelhoefer, H. Kopp, D. Graindorge, L. Margheriti, M. Moretti, S. Murphy, M.A. Gutscher, Crustal structure of the Ionian Basin and eastern sicily margin: results from a wide-angle seismic survey, J. Geophys. Res. Solid Earth 123 (2018) 2090–2114, https://doi.org/10.1002/2017JB015312.

[40] J. Tugend, N. Chamot-Rooke, S. Arsenikos, C. Blanpied, D.F. de Lamotte, Geology of the Ionian Basin and margins: a key to the east mediterranean geodynamics, Tectonics 38 (2019) 2668–2702, https://doi.org/10.1029/2018TC005472.

[41] D. Jongsma, J.E. van Hinte, J.M. Woodside, Geologic structure and neotectonics of the north african continental margin south of sicily, Mar. Petrol. Geol. 2 (1985) 156–179, https://doi.org/10.1016/0264-8172(85)90005-4.

[42] L. Torelli, M. Grasso, G. Mazzoldi, D. Peis, D. Gori, Cretaceous to neogene structural evolution of the lampedusa shelf (pelagian sea, central mediterranean), Terra. Nova 7 (1995) 200–212, https://doi.org/10.1111/j.1365-3121.1995.tb00689.x.

[43] M. Palano, L. Ferranti, C. Monaco, M. Mattia, M. Aloisi, V. Bruno, F. Cannavò, G. Siligato, GPS velocity and strain fields in Sicily and southern Calabria, Italy: updated geodetic constraints on tectonic block interaction in the central Mediterranean, J. Geophys. Res. Solid Earth 117 (2012) B7, https://doi.org/10.1029/2012JB009254.

[44] S. Cirilli, G. Panfili, N. Buratti, A. Frixa, Paleoenvironmental reconstruction by means of palynofacies and lithofacies analyses: an example from the Upper Triassic subsurface succession of the Hyblean Plateau Petroleum System (SE Sicily, Italy), Rev. Palaeobot. Palynol. 253 (2018) 70–87, https://doi.org/10.1016/j.revpalbo.2018.04.003.

[45] M. Grasso, F. Lentini, Sedimentary and tectonic evolution of the eastern Hyblean Plateau (southeastern Sicily) during late Cretaceous to Quaternary time, Palaeogeogr. Palaeoclimatol. Palaeoecol. 39 (1982) 261–280, https://doi.org/10.1016/0031-0182(82)90025-6.

[46] F. Gerardi, A. Smedile, C. Pirrotta, M.S. Barbano, P.M. De Martini, S. Pinzi, A.M. Gueli, G.M. Ristuccia, G. Stella, S.O. Troja, Geological record of tsunami inundations in Pantano Morghella (south-eastern Sicily) both from near and far-field sources, Nat. Hazards Earth Syst. Sci. 12 (2012) 1185–1200, https://doi.org/10.5194/nhess-12-1185-2012.

[47] T. Ohsumi, Y. Dohi, H. Hazarika, Strong motion and tsunami related to the AD 365 crete earthquake, J. Disaster Res. 13 (2018) (2004) 943–956, https://doi.org/10.20965/jdr.2018.p0943.

[48] P.M. De Martini, L. Graziani, A. Maramai, S. Orefice, D. Pantosti, A. Smedile, Tsunamis in the mediterranean sea, Ref. Mod. in Earth Syst. Environ. Sci. 1 (2020) 1–30, https://doi.org/10.1016/B978-0-12-409548-9.11782-8.

[49] A.G. Samaras, T.V. Karambas, R. Archetti, Simulation of tsunami generation, propagation and coastal inundation in the Eastern Mediterranean, Ocean Sci. 11 (2015) 643–655, https://doi.org/10.5194/os-11-643-2015.

[50] E. Guidoboni, G. Ferrari, G. Tarabusi, G. Sgattoni, A. Comastri, D. Mariotti, C. Ciuccarelli, M.G. Bianchi, G. Valensise, CFTI5Med, the new release of the catalogue of strong earthquakes in Italy and in the Mediterranean area, Sci. Data 6 (2019) 80, https://doi.org/10.1038/s41597-019-0091-9.

[51] A. Karkani, N. Evelpidou, M. Tzouxanioti, A. Petropoulos, M. Gogou, E. Mloukie, Tsunamis in the Greek region: an overview of geological and geomorphological evidence, Geosciences 12 (2022) 4, https://doi.org/10.3390/geosciences12010004.

[52] M.S. Barbano, R. Rigano, M. Cosentino, G. Lombardo, Seismic history and hazard in some localities of south-eastern Sicily, Boll. di Geofis. Teor. ed Appl. 42 (2001) 107–120.

[53] Bottone, D., 1718. De immani Trinacriae terraemotu. Idea Historico-Physica, in Qua Non Solum Telluris Concussiones Transactae Recensentur, sed novissimae anni 1717. Messina.

[54] Boccone, P., 1697. Intorno Il Terremoto Della Sicilia Seguito L'anno 1693. Museo di Fisica, Venezia.

[55] A. Polonia, E. Bonatti, A. Camerlenghi, R.G. Lucchi, G. Panieri, L. Gasperini, Mediterranean megaturbidite triggered by the AD 365 Crete earthquake and tsunami, Sci. Rep. 3 (2013) 1285, https://doi.org/10.1038/srep01285.

[56] A. Argnani, C. Bonazzi, Malta Escarpment fault zone offshore eastern Sicily: Pliocene-quaternary tectonic evolution based on new multichannel seismic data, Tectonics 24 (2005) TC4009, https://doi.org/10.1029/2004TC001656.

[57] F. Gallais, D. Graindorge, M.A. Gutscher, D. Klaeschen, Propagation of a lithospheric tear fault (STEP) through the western boundary of the Calabrian accretionary wedge offshore eastern Sicily (Southern Italy), Tectonophysics 602 (2013) 141–152, https://doi.org/10.1016/j.tecto.2012.12.026.
[58] Y. Okada, Surface deformation due to shear and tensile faults in a half-space, Int. J. Rock Mech. Min. Sci. Geomech. Abstr. 23 (1986) 1135–1154, https://doi.org/10.1016/0148-9062(86)90674-1.
[59] Y. Okada, Internal deformation due to shear and tensile faults in a half-space, Bull. Seismol. Soc. Am. 82 (1992) 1018–1040, https://doi.org/10.1785/BSSA0820021018.
[60] R.A. Khan, N.K.R. Kevlahan, Data assimilation for the two-dimensional shallow water equations: optimal initial conditions for tsunami modelling, Ocean Model. 174 (2022), 102009, https://doi.org/10.1016/j.ocemod.2022.102009.
[61] C. Sánchez-Linares, M. de la Asunción, M.J. Castro, S. Mishra, J. Šukys, Multi-level Monte Carlo finite volume method for shallow water equations with uncertain parameters applied to landslides-generated tsunamis, Appl. Math. Model. 39 (2015) 7211–7226, https://doi.org/10.1016/j.apm.2015.03.011.
[62] F.A.T. Laksono, M.R. Aditama, R. Setijadi, G. Ramadhan, Run-up height and flow depth simulation of the 2006 south java tsunami using COMCOT on widarapayung Beach, IOP Conf. Ser. Mater. Sci. Eng. 982 (2020), 012047, https://doi.org/10.1088/1757-899X/982/1/012047.
[63] K. Hu, C.G. Mingham, D.M. Causon, Numerical simulation of wave overtopping of coastal structures using the non-linear shallow water equations, Coast. Eng. 41 (2000) 433–465, https://doi.org/10.1016/S0378-3839(00)00040-5.
[64] Syamsidik, T.M. Rasyif, S. Kato, Development of accurate tsunami estimated times of arrival for tsunami-prone cities in Aceh, Indonesia, Int. J. Disaster Risk Reduc. 14 (2015) 403–410, https://doi.org/10.1016/j.ijdrr.2015.09.006.
[65] A. Geyer, R. Quirchmayr, Shallow water equations for equatorial tsunami waves, Philos. Trans. R. Soc. A Math. Phys. Eng. Sci. 376 (2018), 20170100, https://doi.org/10.1098/rsta.2017.0100.
[66] K. Satake, Tsunamis, in: G. Schubert (Ed.), Treatise on Geophysics, Elsevier, Amsterdam, 2015, pp. 477–504.
[67] Y. Liu, Y. Shi, D.A. Yuen, E.O.D. Sevre, X. Yuan, H.L. Xing, Comparison of linear and nonlinear shallow wave water equations applied to tsunami waves over the China Sea, Acta Geotech 4 (2009) 129–137, https://doi.org/10.1007/s11440-008-0073-0.
[68] K. Lambeck, F. Antonioli, M. Anzidei, L. Ferranti, G. Leoni, G. Scicchitano, S. Silenzi, Sea level change along the Italian coast during the Holocene and projections for the future, Quat. Int. 232 (2011) 250–257, https://doi.org/10.1016/j.quaint.2010.04.026.
[69] G. Scicchitano, E.F.C. Berlinghieri, F. Antonioli, C.R. Spampinato, C. Monaco, Sacred landscapes and changing sea levels: new interdisciplinary data from the early neolithic to the present in South-Eastern Sicily, in: G. Bailey, J. Harff, D. Sakellariou (Eds.), Under the Sea: Archaeology and Palaeolandscapes of the Continental Shelf, Springer, Cham, 2017, pp. 233–253.
[70] F.A.T. Laksono, L. Borzì, S. Distefano, A. Di Stefano, J. Kovács, Shoreline prediction modelling as a base tool for coastal management: the Catania Plain case study (Italy), J. Mar. Sci. Eng. 10 (1988) (2022), https://doi.org/10.3390/jmse10121988.
[71] M. Anzidei, G. Scicchitano, G. Scardino, C. Bignami, C. Tolomei, A. Vecchio, E. Serpelloni, V. De Santis, C. Monaco, M. Milella, A. Piscitelli, G. Mastronuzzi, Relative sea-level rise scenario for 2100 along the coast of south eastern Sicily (Italy) by insar data, satellite images and high-resolution topography, Rem. Sens. 13 (2021) 1108, https://doi.org/10.3390/rs13061108.
[72] A. Sulli, V.L. Presti, M.G. Morticelli, F. Antonioli, Vertical movements in NE Sicily and its offshore: outcome of tectonic uplift during the last 125 ky, Quat. Int. 288 (2013) 168–182, https://doi.org/10.1016/j.quaint.2012.01.021.
[73] F.A.T. Laksono, L. Czirok, L. Borzi, A. Di Stefano, A. Halmai, J. Kovács, Shoreline change dynamics along the Augusta coast, eastern sicily, south Italy, Earth Surf. Process. Landforms (2023) 1–12, https://doi.org/10.1002/esp.5644.
[74] K. Berryman, Review of tsunami hazard and risk in New Zealand, in: Inst. Geol. Nucl. Sci., first ed., Lower Hutt, 2006.
[75] DISS Working Group, Database of individual seismogenic sources (DISS), version 3.1.1, in: A Compilation of Potential Sources for Earthquakes Larger than, M 5.5 in Italy and surrounding areas, 2023. http://diss.rm.ingv.it/diss/.
[76] NOAA, Sea Level Rise Viewer, 2015. https://coast.noaa.gov/digitalcoast/tools/slr.html. (Accessed 5 January 2023).
[77] C. Monaco, F. Antonioli, G. De Guidi, K. Lambeck, L. Tortorici, V. Verrubbi, Tectonic uplift and sea-level change during the holocene in the Catania Plain (eastern sicily), Quat. Nova 8 (2004) 171–185.
[78] F.A.T. Laksono, A. Widagdo, M.R. Aditama, M.R. Fauzan, J. Kovács, Tsunami hazard zone and multiple scenarios of tsunami evacuation route at jetis Beach, cilacap regency, Indonesia, Sustain. Times 14 (2022) 2726, https://doi.org/10.3390/su14052726.
[79] F.A.T. Laksono, L.L.Y. Tsai, J. Pilarczyk, The sedimentological record of Upper Holocene tsunami event in Fengbin, Taiwan, Geopersia 11 (2021) 169–203, https://doi.org/10.22059/geope.2020.301603.648548.
[80] F.A.T. Laksono, Assessment of building vulnerability to tsunami using the PTVA-4 method: case study of the 2006 Cilacap tsunami tragedy, in: W.C. Moon, T. L. Lau (Eds.), Tsunamis: Detection Technologies, Response Efforts and Harmful Effects, Nova Science Publishers, New York, 2022, pp. 1–14, https://doi.org/10.52305/BFIU1020.